DOI 10.1007/s11141-024-10302-1
Radiophysics and Quantum Electronics, Vol. 66, Nos. 5–6, October–November, 2023
(Russian Original Vol. 66, Nos. 5–6, May–June, 2023)

DYNAMICS OF THE SELF-ACTION OF WAVE FIELDS IN MULTICORE FIBERS

A. A. Balakin,* S. A. Skobelev, A. V. Andrianov, and A. G. Litvak

UDC 530.112+537.876.4

We review modern studies of the self-action of laser radiation in discrete systems using the example of multicore fibers. The critical power is shown to exist, at which the self-trapping (the discrete analog of collapse) of radiation occurs even in a one-dimensional lattice of weakly coupled cores. The transition of nonlinear dynamics to the stochastic regime in discrete systems is studied, and the threshold amplitude for this transition is determined. It is shown that the use of a special configuration with a dedicated core in the center of a ring of identical cores makes it possible to control the self-trapping process and apply it for nonlinear radiation filtering and self-compression of laser pulses. It is established that arbitrarily powerful coherent radiation can be handled using stable out-of-phase supermodes, which are wave-field distributions over all fiber cores with a maximum propagation constant. Such out-of-phase supermodes are demonstrated for core configurations shaped as a ring, a line, a square matrix, and a hexagonal structure. The first experiments have already shown the feasibility and stability of the found out-of-phase supermodes, in both fibers with a ring configuration and fibers having a square matrix of cores.

1. INTRODUCTION

Laser systems consisting of a large number of fiber light guides attract great attention as a fairly simple way to create ultrafast optical radiation sources with very high power [1, 2]. The peak power of radiation that can be generated and transported in a common single-core fiber has natural constraints related to the nonlinearity of the fiber material and cannot exceed the critical power of self-focusing. It is reasonable to assume that the total power of a multi-channel fiber system increases just as a function of the number of guides that comprise the system. However, for many tasks requiring an extremely high power it is important to preserve the coherent radiation coupling in all fibers of the array in order to ensure the possibility of summing the multi-channel radiation efficiently into a single optical wave beam and focusing it subsequently. The performed experiments on radiation transportation in systems with few channels demonstrate that securing the phase synchronism of radiation in a large number of independent channels with inevitable random variations in channel parameters requires significant technological efforts related to the development of a feedback system for phase control in each channel [3, 4, 5, 6, 7]. A possible way to solve the phasing problem is to switch over from an array of independent light guides to multicore fibers (MCFs) with weakly coupled cores [8, 9, 10, 11]. In such filters, collective nonlinear modes (supermodes) of coherent radiation may be formed; these supermodes are distributed over many closely-spaced cores and are hardly sensitive to fluctuations in the phases of the beams injected into the system. The total radiation power in this case can exceed by far the radiation power in a single light guide. Moreover, the multicore fibers can themselves

* balakin@ipfran.ru

A. V. Gaponov-Grekhov Institute of Applied Physics of the Russian Academy of Sciences, Nizhny Novgorod, Russia. Translated from Izvestiya Vysshikh Uchebnykh Zavedenii, Radiofizika, Vol. 66, Nos. 5–6, pp. 406–446, May–June 2023. Russian DOI: 10.52452/00213462_2023_66_05_406 Original article submitted May 31, 2023; accepted June 30, 2023.

serve as independent channels for additional synchronization toward an even greater (sevenfold) increase in the transmitted power of the coherent radiation.

The possibility to increase the total power significantly due to the use of MCFs is confirmed by the results of recent studies of nonlinear dynamics in periodic discrete media. A significant difference of nonlinear processes in such media from the ones in continuous media is the possibility of a discrete wave collapse even in the one-dimensional case [12, 13, 14, 15, 16]. This collapse leads to the capture of the initially broad field distribution with a total power exceeding the threshold value into the single node of the system. Another effect which takes place in MCF systems with an in-phase field distribution over all light guides is discrete filamentation instability accompanied with the coherence loss in the transported radiation [16].

It is very important that the effects of discrete collapse and filamentation, which hinder the transportation of intense radiation, are absent in the case of wave beams with the out-of-phase (antiphase) field distribution in adjacent cores. Stable high-intensity field distributions [17, 18, 19, 20, 21], which are also robust with respect to the deformation of the light guide structure [22], can be formed in such MCF systems. This way may be used to generate and transport radiation in MCF system with tightly packed cores; such systems accommodate the peak powers exceeding the threshold power for one core by tens and hundreds of times. High-efficiency self-compression of non-one-dimensional spatiotemporal soliton field distributions with achieved pulse durations comparable with the field period is also possible in out-of-phase MCFs [23].

We prepared this review of nonlinear dynamics of wave beams and packets in MCF systems for publication in the special journal issue dedicated to the 90th anniversary of Vladimir Ilyich Talanov. At the start of the studies in the field of nonlinear optics, V. I. Talanov obtained several essential fundamental results. In particular, he determined the structure of the two-dimensional spatial envelope soliton [24], formulated the nonlinear parabolic equation for wave beams and packets, which was later called the nonlinear Schrödinger equation [25, 26], discovered the effect of self-focusing instability [27], determined the mandatory condition for the wave collapse (self-focusing) of beams with arbitrary intensity profiles [28], and demonstrated the existence of optical solitons and the effects of self-compression of wave packets in media with the Kerr nonlinearity and abnormal dispersion of the group velocity [26]. After essential modification, these fundamental concepts and results play the key part also in the theory of nonlinear wave dynamics in discrete systems as well.

When presenting a comprehensive theoretical analysis of nonlinear dynamics of wave beams and packets in MCF systems, we focus mainly on considering arrays of weakly coupled cores with out-of-phase field distributions, which is the most interesting case for practical applications. The review also includes a brief description of the first experiments on generation and transportation of laser pulses in multicore fiber light guides, these experiments confirming great prospects for the discussed research line.

2. BASIC EQUATIONS

To obtain the discrete equation, we will assume that the fiber cores are identical and so small that only the lowest (fundamental) mode $\phi(x, y)$ is excited in each of them. Then, the field can be represented approximately as the sum,

$$\mathcal{A}(z, \tau, x, y) \approx \sum_n u_n(z, \tau)\, \phi(x - x_n, y - y_n), \tag{1}$$

where u_n and $\mathbf{r}_n = (x_n, y_n)$ are, respectively, the potential amplitude and the center coordinates of the nth core, τ is the time, and the z axis of the Cartesian coordinate system x, y, z is directed along the fiber axis. Assuming that the overlap of the wave fields of the adjacent cores is small (here, $\mathbf{d}$ is the distance between the cores),

$$\int \phi(\mathbf{r})\phi(\mathbf{r} + \mathbf{d})\, \mathrm{d}x\, \mathrm{d}y \ll \int \phi^2(\mathbf{r})\, \mathrm{d}x\, \mathrm{d}y, \tag{2}$$

one can use the variational approximation for the chain of equidistant cores and obtain a set of differential equations for the quasimonochromatic field (1). This set of equations, which are also called the discrete

nonlinear Schrödinger equation (NSE), is written as [14, 29, 30]

$$i\frac{\partial u_n}{\partial z} = \chi(u_{n-1} + u_{n+1}) + \alpha\frac{\partial^2 u_n}{\partial \tau^2} + |u_n|^2 u_n, \tag{3}$$

where χ and α are the coupling and dispersion coefficients, respectively. The equation describes the fiber with normal dispersion at $\alpha < 0$, and the one with abnormal dispersion, at $\alpha > 0$, allowing propagation of soliton-like wave packets. Equation (3) conserves the integrals of motion

$$W = \sum_n \int |u_n|^2 \,\mathrm{d}\tau, \quad H = \sum_n \int \left[\alpha \left|\frac{\partial u_n}{\partial \tau}\right|^2 - \frac{|u_n|^4}{2} - \chi(u_{n+1}u_n^* + u_n u_{n+1}^*)\right] \mathrm{d}\tau,$$

and its action is equal to

$$S = \sum_n \int \frac{1}{2i}\left[\left(u_n^*\frac{\partial_z u_n}{\partial z} - u_n\frac{\partial_z u_n^*}{\partial z}\right) - \alpha\left|\frac{\partial u_n}{\partial \tau}\right|^2 + \frac{|u_n|^4}{2} + \chi(u_{n+1}u_n^* + u_n u_{n+1}^*)\right] \mathrm{d}\tau. \tag{4}$$

It should be noted that the introduction of new variables $z^{\mathrm{new}} = z/\chi$, $\tau^{\mathrm{new}} = \tau\sqrt{\chi}$, and $u_n^{\mathrm{new}} = u_n/\sqrt{\chi}$ allows one to set $\chi = 1$ without loss of generality. Then, the dimensional power $\mathcal{P} = \sum |u_n|^2 \int \phi^2(\mathbf{r})\,\mathrm{d}x\,\mathrm{d}y$ is related to the discrete power $P = \sum |u_n^{\mathrm{new}}|^2$ via the following relationship:

$$\mathcal{P} = \chi P \int \phi^2(\mathbf{r})\,\mathrm{d}x\,\mathrm{d}y \approx P\int \phi(\mathbf{r})\phi(\mathbf{r}+\mathbf{d})\,\mathrm{d}x\,\mathrm{d}y. \tag{5}$$

3. BOUNDLESS MATRIX OF THE CORES

At first glance, the use of fairly wide wave beams propagating in a microstructured medium is the simplest way to handle powers which exceed significantly the critical power $\mathcal{P}_{\mathrm{cr}}$ of self-focusing in a homogeneous medium. Therefore, it makes sense to study the dynamics of wave fields in a fiber consisting of a great (infinite in the limiting case) number of cores coupled weakly with each other. Features of nonlinear dynamics of the wave fields in discrete systems depend weakly on the kind of the core grid. The reason is that the influence of the discreteness becomes noticeable for the fields having characteristic scales equal to the grid period, when the grid dispersion has a similar character in both the one-dimensional (of line cores) and two-dimensional (of matrix cores) cases. Therefore, for simplicity we restrict ourselves to the one-dimensional case when describing the dynamics of self-action in discrete systems. For the sake of simplicity, we use the discrete NSE (3) and assume that the number of cores is large enough, i.e., neglect the boundary effects.

3.1. Discrete collapse

First of all, we study particular features of the self-action of wave beams in a dispersion-free medium ($\alpha = 0$). We recall that, in a homogeneous medium, the self-action leads to the formation of a stable soliton solution in the one-dimensional case [31]. In the discrete case, additionally, self-trapping of radiation in a single core becomes possible; this effect is called coherent summation or discrete collapse [12].

To describe it, we use the variational method and represent the approximate solution as

$$u_n = \sqrt{\frac{P}{\sqrt{\pi}a}}\exp\left(-\frac{n^2}{2a^2} + ibn^2 + i\theta\right), \tag{6}$$

where P is the power of the wave field, and the z-dependent parameters a, b, and θ characterize the width of the wave-beam phase front, its curvature, and the homogeneous field phase, respectively. We substitute Eq. (6) into the action (4) at $\alpha = 0$ and replace the summation with integration assuming that the beams

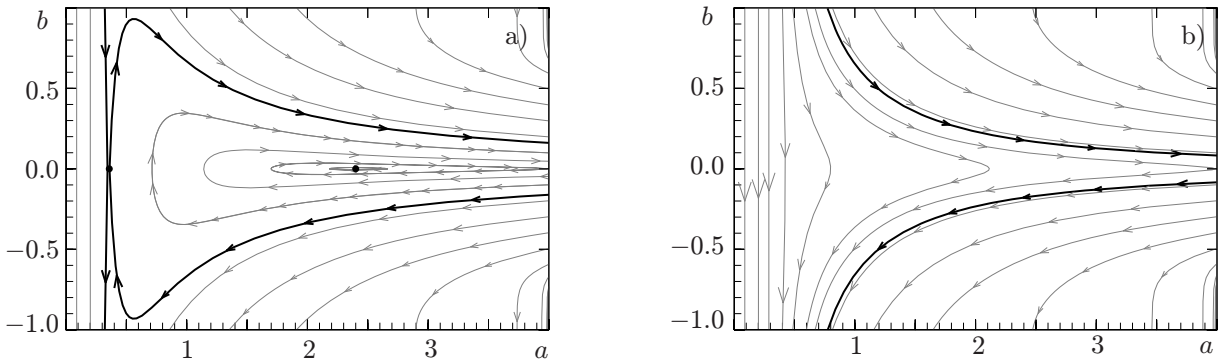

Fig. 1. Phase plane of Eqs. (8) at the powers (*a*) $P = 2$ and (*b*) $P = 5$. The dots mark the equilibrium states. Thick black curves indicate the separatrices, including the curve separating the regions with the localized and unbounded variations in the width a.

are small on the grid scale ($a \gg 1$). As a result, we obtain the expression for the reduced action

$$\bar{S} = \int \left(\frac{P^2}{\sqrt{8\pi}a} + 2P \exp[-b^2a^2 - 1/(4a^2)] - \frac{Pa^2}{2}\dot{b} - P\dot{\theta} \right) \mathrm{d}z. \tag{7}$$

Here, the overdot denotes differentiation with respect to the z coordinate.

Varying the reduced action (7) yields the equations for the solution parameters,

$$\dot{a} = 4ba \exp[-b^2a^2 - 1/(4a^2)], \quad \dot{b} = \left(\frac{1}{a^4} - 4b^2 \right) \exp[-b^2a^2 - 1/(4a^2)] - \frac{P}{\sqrt{8\pi}a^3}. \tag{8}$$

The factor $\exp[-b^2a^2 - 1/(4a^2)]$ reveals specific features of the discrete problem. In the continuum limit $a \gg 1$, $ba \ll 1$, it is close to 1. In the opposite case, it yields the exponentially fast attenuation of the diffraction of the wave beams having the width close to the grid period ($a \lesssim 1$).

Equations (8) are most easily analyzed through the phase plane (Fig. 1). They have up to three stationary points (a_*, b_*) at

$$a_* = \infty \quad \text{or} \quad P = \frac{\sqrt{8\pi}}{a_*} \exp[-1/(4a_*^2)], \quad b_* = 0. \tag{9}$$

At $P \le P_\mathrm{m} = 4\sqrt{\pi/e} \approx 4.3$, there are three stationary points: (i) the saddle point at $a_* = \infty$ yields a separatrix separating transit and periodic motions, (ii) the middle equilibrium state of the center type at $a_* \propto 1/P$ is stable (Fig. 1*a*) and corresponds to the soliton in the continuum limit, and (iii) the saddle point at $a_* \propto 1/\sqrt{\ln(\sqrt{8\pi}/P)} \sim 1$ separates strongly localized solutions at small a. The limiting value $P = P_\mathrm{m}$ corresponds to the solution with the width $a_* = 1/\sqrt{2}$ comparable with the grid period. The fundamental differences from the continuum case appear at the powers $P > P_\mathrm{m}$, when only the stationary saddle-type point at infinity remains and the discrete collapse of the radiation (trapping in one core) occurs (Fig. 1*b*). In dimensional variables, the obtained limiting power is much lower (in terms of the smallness parameter (2)) than the critical power of self-focusing in the medium.

Numerical simulation of Eq. (3) at $\alpha = 0$ confirms the results of qualitative analysis (Fig. 2). The calculations are performed for a fiber consisting of 100 weakly coupled cores located in line. Zero boundary conditions were used, corresponding to the absence of the cores besides the ones considered. Strongly localized solutions with a relatively low power blur as the amplitude decreases (Fig. 2*a*). Wider initial distributions are characterized by periodic variations in the width and amplitude of the wave field (Fig. 2*b*) similar to the multisoliton dynamics in the continuum limit. At an even greater width of the initial distribution, the radiation power exceeds the threshold value, and the wave field is trapped in one core (Fig. 2*c*). In the case of an exceedingly wide initial distribution with power exceeding the threshold one by many times, the discrete analog of the filamentation instability develops (Fig. 2*d*), which is discussed further in Sec. 3.2.

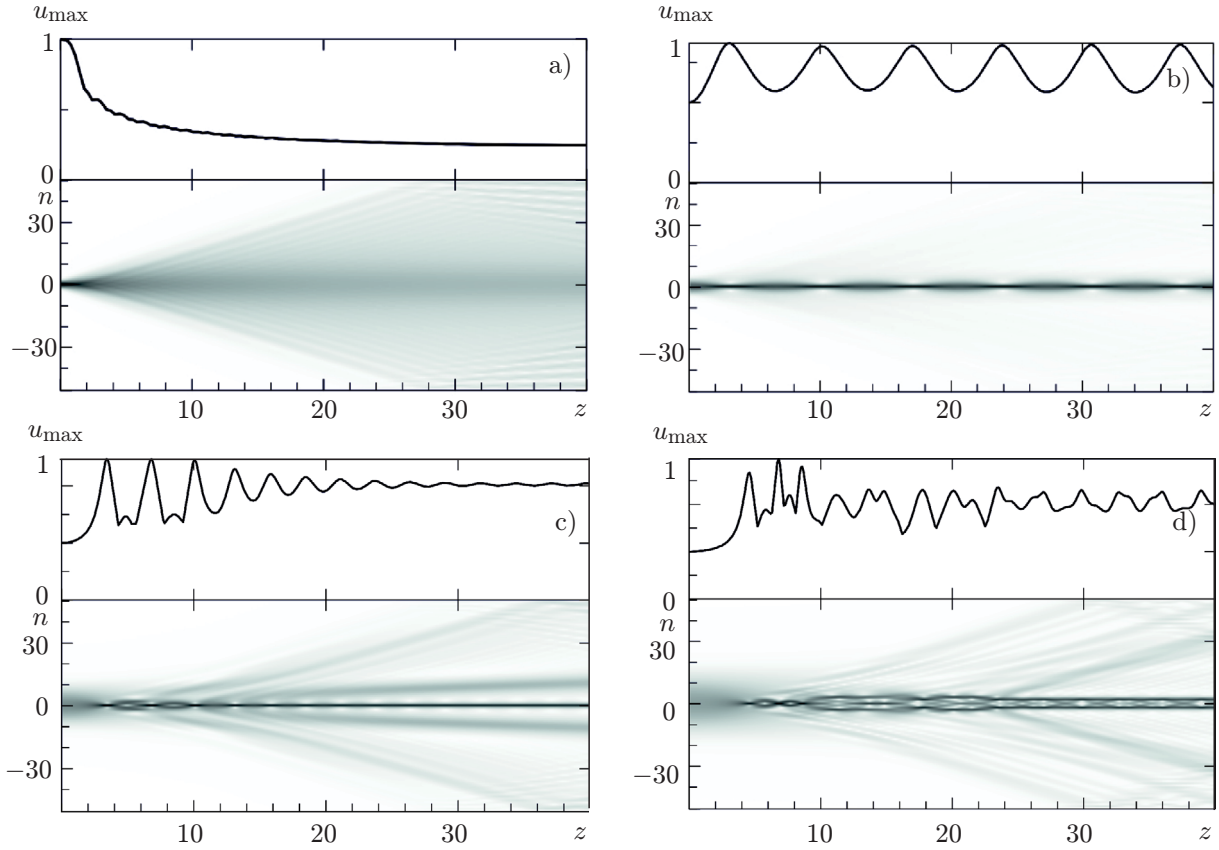

Fig. 2. Dynamics of the wave field with the initial Gaussian distribution $u_n = \exp[-n^2/(2a^2)]$ with (*a*) $a = 1$, $P = 1.8$; (*b*) $a = 2$, $P = 3.5$; (*c*) $a = 4$, $P = 8.9$; (*d*)$a = 8$, $P = 14.2$. The color intensity indicates the field amplitude from zero (white) to the maximum value (black).

3.2. Stochastic dynamics

The results obtained above within the framework of the variational approximation are confirmed by numerical simulations of Eq. (3) only at a not-so-large exceeding of the wave beam power over the threshold value. A further increase in power up to a level exceeding significantly the threshold value results in the wave field splitting and the field narrowing in the self-action process being suppressed. The reason for this is the discrete analog of the filamentation instability [16].

We find the increment of this instability for the homogeneous solution $u_n = u_0 \exp[-i\,(|u_0|^2 + 2)\,z]$ of Eq. (3) at $\alpha = 0$. To this end, we linearize the increment with respect to the low amplitude $|\delta u| \ll |u_0|$ of the perturbed solution $u = [u_0 + \delta u \exp(i\kappa n)] \exp[-i\,(|u_0|^2 + 2)\,z]$

$$i\frac{\partial \delta u}{\partial z} = [\exp(i\kappa) + \exp(-i\kappa) - 2]\,\delta u + |u_0|^2 \delta u + u_0^2 \delta u^*.$$

Adding the complex-conjugate equation, we obtain the exponential growth $\{\delta u, \delta u^*\} \propto \exp(\Gamma z)$ with the increment

$$\Gamma^2 = 4\sin^2(\kappa/2)\left[2\,|u_0|^2 - 4\sin^2(\kappa/2)\right]. \tag{10}$$

It is seen from the obtained expression that the increment maximum is achieved for $\kappa = \pi$ at $|u_0| \geq \sqrt{2}$, i.e. for the perturbations with the period of the light guide grid being $L_\perp \equiv \pi/\kappa = 1$. Therefore, a rather intense wave beam with the amplitude $u_{\max} \gg \sqrt{2}$ disintegrates into a set of structures localized in individual cores. The fields in each core have their own nonlinear shifts of the wave number $h \propto |u_n|^2$ according to Eq. (3). The interaction between the adjacent cores is exponentially weak if the phase difference for the characteristic

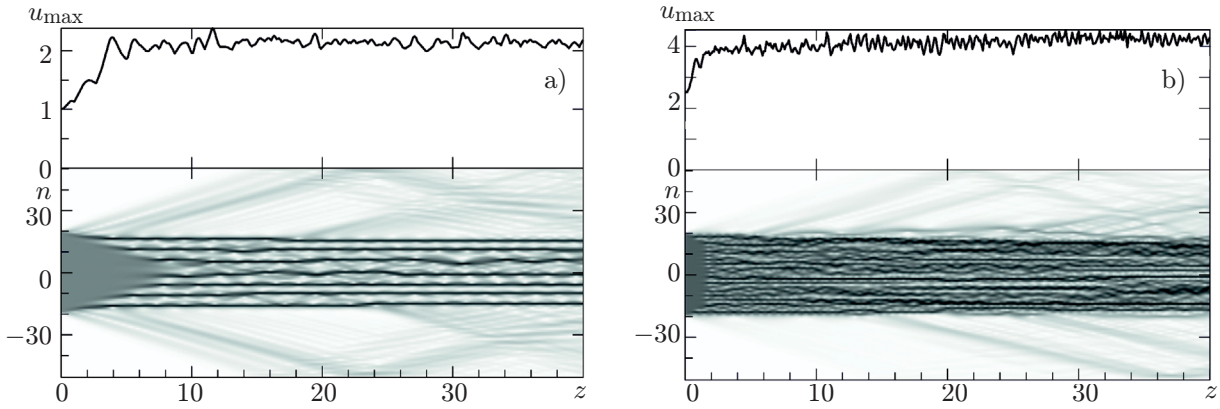

Fig. 3. Dynamics of the wave field with the step-shaped initial distribution at (*a*) $u_0 = 1$, $P = 39$ and (*b*) $u_0 = 2.5$, $P = 244$. The initial noise level is 10^{-3}. The color intensity indicates the field amplitude from zero (white) to the maximum value (black).

width $a \sim L_\perp/2$ of each peak is much greater than π. At the nonlinear stage, this limits the increase in the field amplitude,

$$\frac{L_\perp}{2}\left|u_{\max}^2 - |u_n|^2\right| \gtrsim \pi \quad \Longrightarrow \quad u_{\max} \sim \sqrt{2\pi + |u_0|^2} \geq \sqrt{2\pi}. \tag{11}$$

Numerical simulation confirms this limitation (see Fig. 2*d* and Fig. 3).

The rise of stochastic dynamics results immediately in the loss of radiation coherence between the cores. This makes it impossible to transport the in-phase distribution of the wave field with high power in some part of the cores since the field amplitude threshold in each core is limited by the small value (2), so that the total power is bounded by values much lower than the critical self-focusing power $\mathcal{P}_{\rm cr}$. For example, according to Eq. (5), the threshold power $P_{\rm m} \approx 4.3$ is $\mathcal{P}_{\rm m} \approx 0.01$ MW in dimensional form, and the transition to the stochastic dynamics occurs at the power in the cores above 0.02 MW for fused silica ($\mathcal{P}_{\rm cr} \approx 2.7$ MW [32]) and the coupling length $2\pi/\chi = 100\lambda$, where λ is the wavelength. This leads to the problem of searching for stable wave field distributions engaging all cores of the fiber.

4. RING-SHAPED CONFIGURATION OF THE CORES

It has been shown in the previous section that the use of localized distributions of the wave field in multicore fibers with an infinitely large number of the cores has no prospects from the viewpoint of coherent transportation of radiation with a total power exceeding the critical power $\mathcal{P}_{\rm cr}$ of self-focusing in a homogeneous medium. A natural approach is to switch to fibers with a large but finite number of cores and seek the solutions distributed over all cores of the fiber. A simplest analogy of an infinite chain is a configuration of an even number $2N$ of identical cores arranged in a circle. For the ring configuration of the cores, Eq. (3) should be supplemented with the boundary conditions

$$i\frac{\partial u_n}{\partial z} = u_{n+1} + u_{n-1} + |u_n|^2 u_n + \alpha\frac{\partial u_n}{\partial \tau^2}, \quad u_0 = u_{2N}. \tag{12}$$

4.1. Out-of-phase supermode

We start analyzing Eq. (12) with the beam problem ($\alpha = 0$). In the linear case ($|u_n|^2 \ll 1$), since the equation is homogeneous, it is convenient to seek the solution as a decomposition over the Bloch functions,

$$u_n(z) = \sum_m f_m(z)\exp(i\varkappa_m n), \quad \varkappa_m = \pi m/N. \tag{13}$$

Substituting Eqs.(13) into Eqs. (12), we obtain equations for the amplitudes of supermodes[1] $f_m(z)$ with the simple solution,

$$i\frac{\partial f_m}{\partial z} = 2f_m \cos\varkappa_m, \qquad f_m(z) = \exp[-2i\cos(\varkappa_m)\, z] f_m(0). \tag{14}$$

Formally, the supermodes (14) are still exact solutions in the nonlinear case for the arbitrary amplitude f_m,

$$u_n = f_m \exp(i\varkappa_m n - ih_m z), \quad h_m = 2\cos\varkappa_m + |f_m|^2. \tag{15}$$

and only the eigen wave number h_m of the supermode changes in this case. However, almost all of these solutions are unstable with respect to azimuthal perturbations.

Indeed, substituting the wave field by a superposition of solution (15) and the small perturbation $\delta_l \exp(i\varkappa_l n)$,

$$u_n = \left[f_m \exp(i\varkappa_m n) + \delta_l \exp(i\varkappa_l n)\right] \exp(-ih_m z), \quad \{l, m\} = 0, \ldots, 2N-1, \quad |\delta_l| \ll |f_m|,$$

into Eqs. (12) at $\alpha = 0$ and linearizing with respect to small perturbations, we obtain the following equation for δ_l in the first order of smallness:

$$i\frac{\mathrm{d}\delta_l}{\mathrm{d}z} = 2\delta_l(\cos\varkappa_l - \cos\varkappa_m) + f_m^2\delta_l^* + |f_m|^2\delta_l. \tag{16}$$

Considering solution of Eq. (16) in the form $\{\delta_l,\, \delta_l^*\} \propto \exp(\Gamma z)$, we obtain an algebraic set of two homogeneous equations, which have a nontrivial solution at Γ satisfying the dispersion relation

$$\Gamma^2 = |f_m|^4 - \left[2\,(\cos\varkappa_l - \cos\varkappa_m) + |f_m|^2\right]^2. \tag{17}$$

The perturbations do not increase at $\Gamma^2 \le 0$. This condition can be fulfilled for all wave numbers $\varkappa_l$ of the perturbations and all amplitudes f_m only at $\varkappa_m = \pi$. Correspondingly, only such supermode called "out-of-phase supermode" [17]

$$u_n = (-1)^n \exp[i\,(2 - |f_N|^2)\, z]\, f_N, \tag{18}$$

is stable at any amplitude f_N. Moreover, its intensity $|u_n|^2 = f_N^2$ is distributed homogeneously over all fiber cores. Therefore, the use of the out-of-phase (antiphase) supermode allows one to increase the transported power of the wave field by up to $2N$ times compared with the case of single-core fiber. This makes the out-of-phase distribution (18) most promising for coherent transportation of the radiation in multicore fibers.

It should be noted that if $m \neq N$, solutions (15) are also stable at low amplitudes $|f_m|^2 \le \cos\varkappa_m - \cos\varkappa_{m+1}$. For example, the in-phase supermode ($m = 0$) is stable only for the amplitudes $|f_0|^2 \le 2 - 2\cos(\pi/N) = 4\sin^2[\pi/(2N)]$. For a large number of cores ($N \gg 1$), this yields a rather small value $|f_0|^2 \le \pi^2/N^2 \ll 1$, making it impossible to handle large radiation power in the in-phase supermode.

4.2. Bent fiber

In Sec. 4.1, we found the out-of-phase distribution of the wave field and demonstrated its stability with respect to small perturbations. However, the issue remains whether the out-of-phase supermodes exist and are stable in multicore fibers with deformed structures. To answer this question, Eqs. (12) should be supplemented with terms related to inhomogeneities in the propagation constants h_n for each core [22]

$$i\frac{\partial u_n}{\partial z} = u_{n-1} + u_{n+1} + |u_n|^2 u_n + h_n u_n, \quad h_n = D\sin(\pi n/N). \tag{19}$$

[1] Here and in what follows, the term "supermodes" denotes the distributions of the wave field that correspond to the eigenmodes of the discrete linear problem.

Here, D is the amplitude of the perturbations of the typical form from fiber bends, where the propagation constant increases proportionally to the distance from the bend center (radius). The equation conserves the power $P = \sum |u_n|^2$.

As a rule, large-scale fluctuations result in excitation of all linear supermodes of the fiber and make the problem difficult to consider analytically. However, if the value D is not too great, the excitations of the out-of-phase supermode remain small, and the approximate solution of Eqs. (19) for $N \geq 2$ can be sought in the form

$$u_n = f_N \exp[i\,(2 - f_N^2)\,z]\,[(-1)^n + \delta_n]\,, \quad |\delta_n|^2 \ll 1. \tag{20}$$

Using this, we find that for the stationary solution in the first order of smallness with respect to $\delta_n \propto h_n$

$$(f_N^2 - 2)\,\delta_n \approx D(-1)^n \sin(\pi n/N) + \delta_{n+1} + \delta_{n-1} + 3f_N^2\delta_n, \quad \delta_n \approx -D\frac{(-1)^n \sin(\pi n/N)}{4\sin^2[\pi/(2N)] + 2f_N^2}. \tag{21}$$

We took into account here that, for real D, f_N and δ_n can be also assumed real without loss of generality. As seen, the perturbations of the solution remain small ($|\delta_n|^2 \ll 1$) while the perturbation of the refraction index is small: either $D \ll 4\sin^2[\pi/(2N)] \leq 2$ or $D \ll 2f_N^2$. The fraction of the power in the perturbed part is the value of the next order of smallness due to the orthogonality of the perturbations and the supermode $(-1)^n$,

$$\frac{\delta P}{P} = \frac{D^2}{2\,\{4\sin^2[\pi/(2N)] + P/N\}^2}. \tag{22}$$

The comparison with the exact solution shows that expression (22) yields the upper estimate of the power fraction in the perturbations (Figs. 4*a*, 4*c*, 4*e*, and 4*g*).

Equation (21) for the perturbation amplitude allows one to find the maximum field intensity $I_{\max} = \max |u_n|^2$ at a given power. The maximum intensity is an important characteristic that provides an estimate for the maximum transported power below the fiber damage. Indeed, the power in each core should not exceed the critical power $\mathcal{P}_{\rm cr}$ of the self-focusing. Then, the total power should be greater for distributions close to homogeneous ones, where the ratio $P/I_{\max}$ is great. For small perturbations ($|\delta_n| \ll 1$), the maximum intensity is approximated well by formula [22]

$$I_{\max} = \max_n |u_n|^2 \approx f_N \max_n |1 + 2\delta_n| = \frac{P}{2N}\left(1 + 2\max_n |\delta_n|\right). \tag{23}$$

Using solution (21), we obtain the simple estimate

$$\frac{P}{I_{\max}} \approx \frac{2N}{1 + \dfrac{2D\cos[\pi/(2N)]}{4\sin^2[\pi/(2N)] + P/N}} \underset{N\gg 1}{\approx} \frac{2N}{1 + 2ND/P}. \tag{24}$$

Figures 4*b*, 4*d*, 4*f*, and 4*h* show the dependence of the maximum intensity $I_{\max}$ on the bending coefficient D and the total power P, the dependence found exactly and based on the approximate solution (24). As seen, they agree well even beyond the applicability of the approximate solution. In the case of strong bending ($D \gg N$, $P \ll DN$), the field is localized in a small number of cores only corresponding to a large value of $I_{\max}$. In the case of high-power radiation ($P \gg DN$), the medium nonlinearity weakens the influence of the fiber deformation, and the maximum intensity decreases [22].

It should be noted that the out-of-phase distribution in a fiber with a bending perturbation $h_n \propto \sin(\pi n/N)$ of the refraction index excites half of the linear supermodes in the ring-shaped configuration. Moreover, the equation set for the amplitudes of these supermodes becomes algebraic since only stationary solutions are of interest. Therefore, it is possible to obtain exact out-of-phase solutions at the arbitrary perturbation amplitude D for not-too-large N [22]. However, it turns out that the asymptotic solution (21) also describes well the out-of-phase distribution at relatively large perturbations.

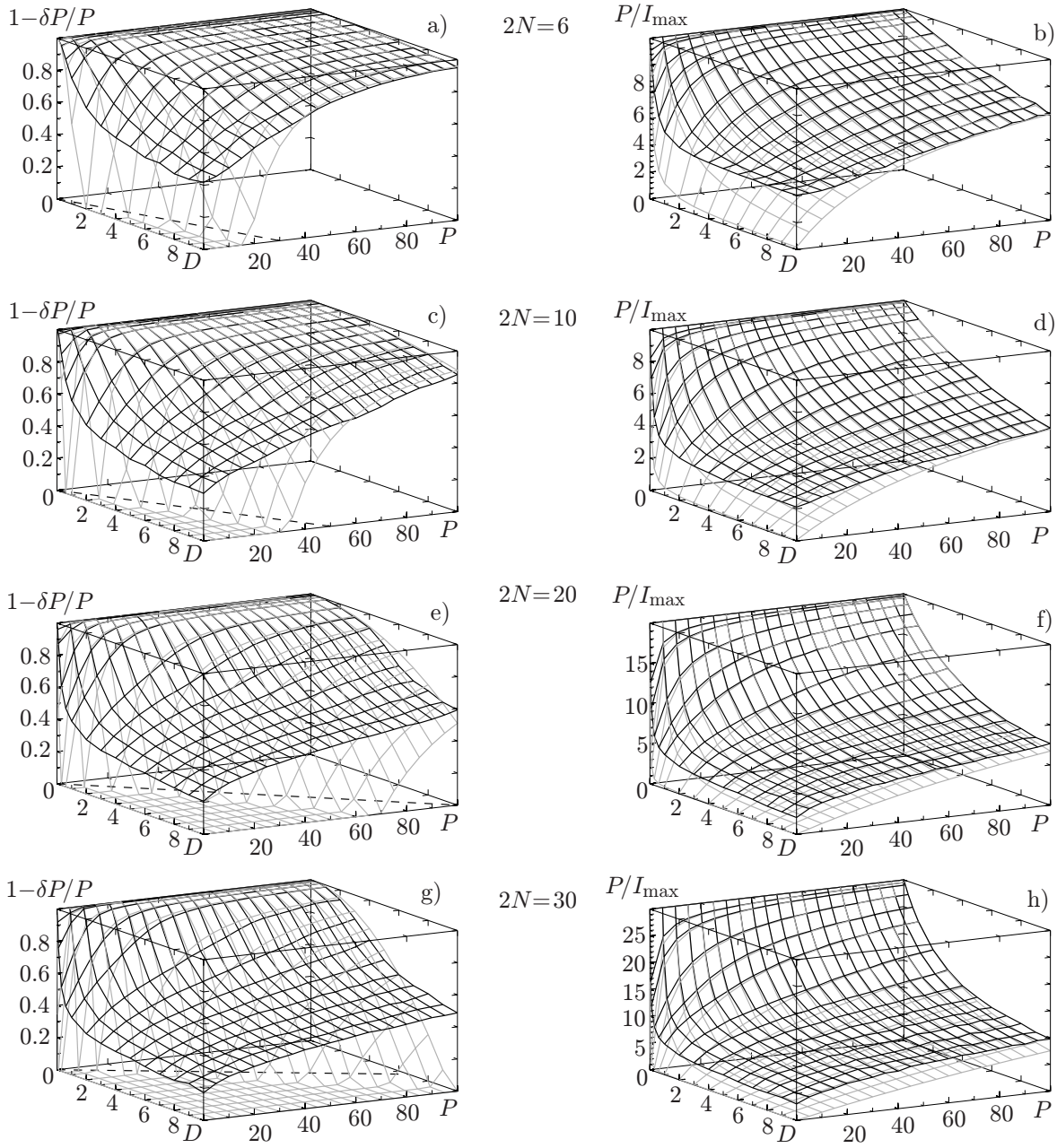

Fig. 4. Power fraction in the out-of-phase supermode (left-hand column) and the maximum intensity $I_{\max}$ (right-hand column) as functions of the perturbation amplitude D and the total power P at different numbers $2N$ of cores. Exact solutions and their asymptotics (22) and (24) are shown in black and gray, respectively. The dashed line corresponds to the boundary $P = DN$.

The presence of amplification inhomogeneity in active fibers changes the pattern qualitatively. We start with studying the stability of the out-of-phase distribution in the active cores, which are described by the equation

$$i\frac{\partial u_n}{\partial z} = i\gamma_n u_n + u_{n-1} + u_{n+1} + |u_n|^2 u_n. \tag{25}$$

The out-of-phase supermode has the same amplitude in all the cores. Therefore, the homogeneous amplification with the coefficient $\gamma = \sum \gamma_n/(2N)$ does not affect the mode stability. To verify this fact, we study the stability of the out-of-phase supermode with respect to the process of linear amplification in the fiber. The main difficulty here comes from the form of the unperturbed solution $u_n^{\mathrm{sol}} = (-1)^n f_N \exp\{\gamma z + 2iz -$

$i\,|f_N|^2\exp(2\gamma z)/(2\gamma)\}$. Therefore, we seek the perturbed solution of the equation in the form [33]

$$u_n = [(-1)^n + \delta u_n]\, f_N \exp\left\{\gamma z + 2iz - i\,|f_N|^2\exp(2\gamma z)/(2\gamma)\right\}, \quad |\delta u_n|^2 \ll 1. \tag{26}$$

For the perturbations $\delta u_n = \sum \delta_k \exp(i\varkappa_k n)$, we obtain the equation

$$i\frac{\partial \delta_k}{\partial z} - 2\delta_k = |f_N|^2\exp(2\gamma z)(\delta_k + \delta_k^*) + 2\delta_k\cos\varkappa_k + \frac{i}{2N}\sum_m \tilde{\gamma}_m(-1)^m\exp(-i\varkappa_k m), \tag{27}$$

where $\tilde{\gamma}_n = \gamma_n - \gamma$. If the amplification coefficients in all the light guides are identical ($\tilde{\gamma}_n = 0$), one can use the local dispersion relation for $\delta_k \propto \exp(i\lambda z)$ at $\gamma \ll 1$ [33],

$$\lambda^2(z) \approx 8\cos^2\left(\frac{\varkappa_n}{2}\right)\left[2\cos^2\left(\frac{\varkappa_n}{2}\right) + f_N^2\exp(2\gamma z)\right] \geq 0. \tag{28}$$

This dispersion relation yields that the perturbations do not grow faster than the amplitude of the out-of-phase supermode since the out-of-phase supermode is stable in the case of the active fiber too [33].

If there is a spread in the amplification coefficient in the cores ($\tilde{\gamma}_n \neq 0$), the forced solution of Eq. (27) has the form

$$\delta u_n \approx -\frac{i}{2N}\sum_m\sum_{k\neq N}\frac{\tilde{\gamma}_m(-1)^m\exp[i\varkappa_k\,(n-m)]}{4\cos^2(\varkappa_k/2)}. \tag{29}$$

It is apparent that the perturbations remain small ($|\delta u_n|^2 \ll 1$), while the perturbation of the amplification coefficient is small, $|\tilde{\gamma}_n| \leq 4\sin^2[\pi/(2N)]$.

4.3. Out-of-phase solitons

It was shown in the previous subsections that the out-of-phase supermode (18) is stable with respect to both small perturbations of the initial conditions and small structure deformations of the multicore fiber, including the case of active fibers. Since the soliton solution exists in the media with abnormal dispersion of the group velocity and focusing nonlinearity ($\alpha > 0$ in Eq. (3)), we will confine ourselves to this case and reduce the equation to the dimensionless form

$$i\frac{\partial u_n}{\partial z} = u_{n-1} + u_{n+1} + \frac{\partial^2 u_n}{\partial \tau^2} + |u_n|^2 u_n. \tag{30}$$

The out-of-phase soliton solution of Eq. (30) [33] is

$$u_n(z,\tau) = (-1)^n\frac{\sqrt{2}b\exp[i\,(2-b^2)\,z]}{\cosh(b\tau)}. \tag{31}$$

To prove that manifold (31) is stable, we use Lyapunov's second method, according to which the manifold of the solutions is stable, if one manages to find the Lyapunov functional $\mathcal{F}[u]$ that satisfies the following requirements: (i) it is positive or equal to zero ($\mathcal{F}[u] \geq 0$); (ii) its derivative is negative or equal to zero ($\mathrm{d}\mathcal{F}/\,\mathrm{d}z \leq 0$); and (iii) it becomes zero only at the given manifold ($\mathcal{F}[u_s] = 0$).

Equation (30) retains the Hamiltonian H and the energy W

$$H = \sum_{n=1}^{2N}\int\left[\left|\frac{\partial u_n}{\partial\tau}\right|^2 - \frac{|u_n|^4}{2} - u_n u_{n+1}^* - u_{n+1}u_n^*\right]\mathrm{d}\tau, \quad W = \sum_{n=1}^{2N}\int|u_n|^2\,\mathrm{d}\tau. \tag{32}$$

The Hamiltonian H is well suited to act as the Lyapunov functional, but it is not bounded from below formally. Indeed, the increase in the field due to the perturbation can lead to amplification of the nonlinear

term and to a decrease in the value of H. Let us use the Lagrange multiplier method to find the minimum of the Hamiltonian H in the class of functions conserving the energy. The first variation of the functional $R[u] = H[u] + \lambda W[u]$ with respect to u_n^* yields the equation

$$\frac{\partial^2 u_n}{\partial \tau^2} + |u_n|^2 u_n + (u_{n+1} - 2u_n + u_{n-1}) - \lambda u_n = 0 \tag{33}$$

for the soliton manifolds (here, $\lambda_m = \lambda - 2\cos\kappa_m$)

$$u_n^{(m)} = \exp(i\kappa_m n)\frac{\sqrt{2\lambda_m}}{\cosh\sqrt{\lambda_m}\tau}, \quad W^{\rm sol} = 8N\sqrt{\lambda_m}. \tag{34}$$

The Hamiltonian for this solution is equal to

$$H_m^{\rm sol} = -16N\sqrt{\lambda_m}\cos\kappa_m - \frac{8N}{3}\lambda_m^{3/2} = -2W\cos\kappa_m - \frac{W^3}{192N^2}. \tag{35}$$

Then, the conditions $\mathcal{F}_m[u_n^{\rm sol}] \geq 0,\ \mathrm{d}\mathcal{F}_m[u]/\,\mathrm{d}z = 0$ are fulfilled for the functional

$$\mathcal{F}_m[u] = \left(H[u] + \frac{W[u]^3}{192N^2} + 2W[u]\cos\kappa_m\right)^2. \tag{36}$$

The main difficulties are related here to proving the uniqueness of the functional zero, i.e., proving that the functional vanishes only at the solution Eq. (34) and nowhere else.

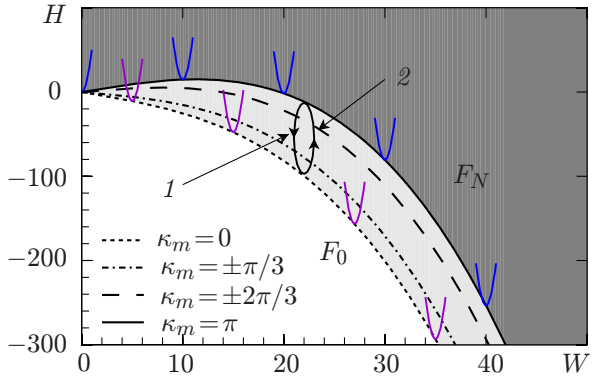

Fig. 5. Hamiltonian H (Eq. (32)) as a function of the energy W. The curves correspond to the extrema (35) at $N = 3$ and various values of m. The arrows indicate the qualitative explanation of the instability at $m = 0$: an increase in (*1*) $|u_m|^2$ or (*2*) $|\kappa_m|$.

Consider, e.g., the solution at $\kappa_m = 0$. A greater difference in the intensities in the cores results in an increase in the nonlinear term and, therefore, to a decrease in the Hamiltonian H (Eq. (32)). This variation of the Hamiltonian is counterbalanced easily by the decrease in the term describing the coupling between the cores (e.g., due to the phase difference arising from the field decay, see Fig. 5). As a result, different distributions correspond to the same values of H and W, i.e., $\mathcal{F}_0 = 0$. Thus, the in-phase solution is unstable and tends to beating with radiation trapping in a single core. Contrariwise, the Hamiltonian for the solution for $\kappa_m = \pi$ always exceeds the one for $\kappa_m < \pi$. This means that the distribution with $\kappa_m = \pi$ cannot disintegrate into distributions with smaller κ_m. Therefore, the increase in the nonlinear term at $\kappa_m = \pi$ cannot be counterbalanced and results in $\mathcal{F}_N > 0$, i.e., the out-of-phase distribution of the wave field is stable [33].

4.4. Ultrashort solitons

Veering onto extremely short pulse durations requires considering the unidirectional wave equation, which has the following form in a medium without high-frequency dispersion [23]:

$$\frac{\partial^2 U_n}{\partial z \partial \tau} + \sigma U_n - X\left(U_{n-1} + U_{n+1}\right) + \frac{\partial^2}{\partial \tau^2}\left(|U_n|^2 U_n\right) = 0. \tag{37}$$

Here, $X > 0$ and σ are, respectively, the coefficients of coupling and low-frequency dispersion, which are related to the corresponding coefficients $\chi = X/\omega_0$ and $\alpha = \sigma/\omega_0^3$ of Eq. (3) in the quasimonochromatic limit

$$U_n = \frac{u_n}{\sqrt{\omega_0}} \exp(i\omega_0\tau), \quad \left|\frac{\partial u_n}{\partial \tau}\right| \ll \omega_0 |u_n|.$$

A specific feature of Eq. (37) is that the coupling between the cores not only yields the phase incursion (same as in Eq. (3)), but also changes the low-frequency dispersion. This feature allows one to vary the effective dispersion of the fiber by using different field distributions in the cores and, e.g., produce easily a fiber with two point of zero dispersion for efficient conversion of the soliton frequency through the Raman scattering [34].

Equation (37) has a solution in the form of a solitary wave which is similar to the out-of-phase soliton (31) [23],

$$U_n(z,\tau) = \frac{(-1)^n}{\sqrt{v}} f(\xi) \exp[i\omega\,(\tau + z/v) + i\int g(\xi)\,\mathrm{d}\xi], \quad \xi = \omega\,(\tau - z/v). \tag{38}$$

Here, ω and v are the characteristic carrier frequency and group velocity of the soliton, respectively. The phase and group velocities of the soliton are not equal; this leads to oscillations of the wave structure, which is most evident for few-cycle laser pulses. Substituting solution (38) into Eq. (37) and separating the real and imaginary parts, one gets equations for the envelope $f(\xi)$ of the soliton and the nonlinear wave number $g(\xi)$:

$$(3f^2 - 1)f'' + 6ff'^2 + (f - f^3)g^2 - 2f^3 g - f^3 - f + \zeta f = 0, \tag{39a}$$

$$(f^3 - f)g' + (6f^2 - 2)f'g + 6f^2 f' = 0. \tag{39b}$$

Here, the prime superscript denotes the derivative according to ξ, and $\zeta = (\sigma + 2X)v/\omega^2 \geq 1$. The case $\zeta = 1$ corresponds to the dispersion relation for Eq. (37) at $f \to 0$. On the soliton solution, the abnormal dispersion should counterbalance the nonlinear phase incursion, which implies the condition $\zeta > 1$.

Equation (39b) is easily reducible to the total derivative, which yields the relation between the functions g and f,

$$g = \frac{(3 - 2f^2)\,f^2}{2\,(1 - f^2)^2}. \tag{40}$$

Substituting it into Eq. (39a) for the real part, we obtain the closed equation for the function f,

$$(1 - 3f^2)f'' - 6ff'^2 - \zeta f + \frac{(2 - f^2)(2 - 3f^2)}{(1 - f^2)^3} = 0. \tag{41}$$

Its Hamiltonian that corresponds to the soliton solution, i.e., the separatrix on the phase plane of the equation (Fig. 6*a*) is equal to

$$H = 4(1 - 3f^2)f'^2 - f^2(2 - 3f^2)\left[2\zeta - \frac{2 - 3f^2}{(1 - f^2)^2}\right]. \tag{42}$$

Since the value of ζ is close to 1 in the quasimonochromatic limit (i.e., for long pulses), it is convenient to introduce the parameter $1/\tau_p^2 = \zeta - 1 > 0$ and rewrite the Hamiltonian as

$$H = 4(1 - 3f^2)f'^2 - \mathcal{U}, \quad \mathcal{U} = f^2(2 - 3f^2)\left[\frac{2}{\tau_p^2} - f^2\frac{1 - 2f^2}{(1 - f^2)^2}\right]. \tag{43}$$

Using this, we obtain the solution by quadrature for the soliton amplitude,

$$\int \frac{1 - 3f^2}{f\sqrt{(1 - 3f^2/2)\{1/\tau_p^2 - f^2(1 - 2f^2)/[2(1 - f^2)^2]\}}}\,\mathrm{d}f = \pm(\xi - \xi_0), \tag{44}$$

with the only parameter τ_p. In the limit of small $f^2 \lesssim 2/\tau_\mathrm{p}^2 \lll 1$, this solution turns into the expression for

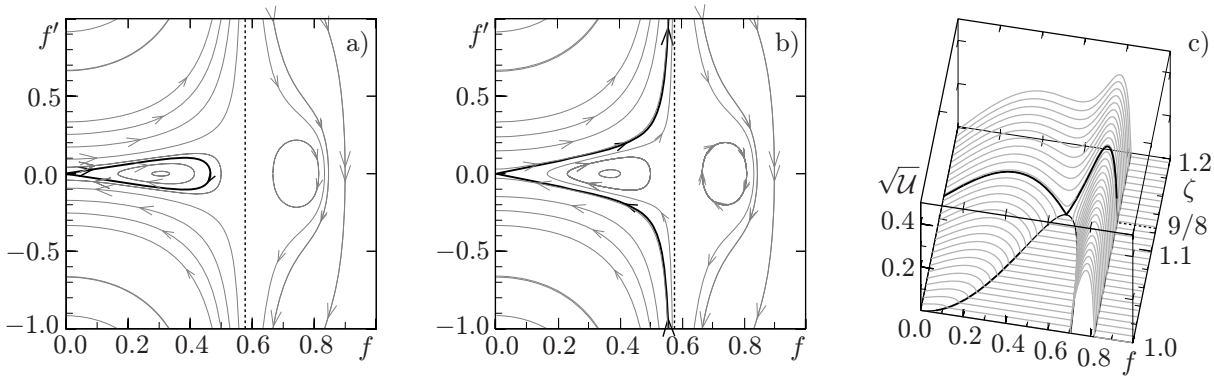

Fig. 6. Phase planes of Eq. (41) at (*a*) $\zeta = 1.1$ and (*b*) $\zeta = 1.15$. The dashed lines mark the singularity at $f = 1/\sqrt{3}$. The bold lines indicate the separatrices. The shape of the potential $\mathcal{U}$ as a function of f at different values of the parameter ζ is shown in panel (*c*).

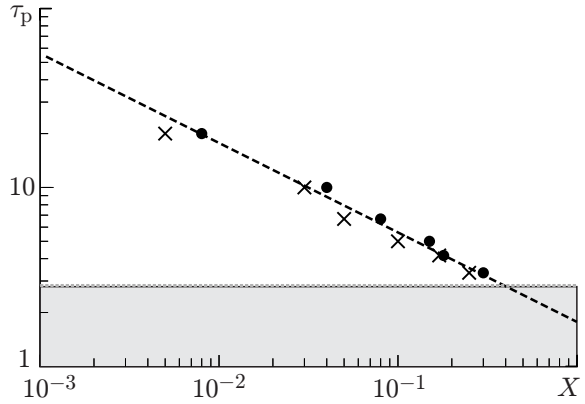

Fig. 7. The threshold value of the coupling coefficient (45) as a function of the soliton parameter τ_p at $\omega = 1$ and $\sigma = 1$. The dots mark the parameters of the stable solutions, and the crosses correspond to the unstable propagation regime. The dashed line shows the dependence $X = \pi/\tau_\mathrm{p}^2$. The shaded region indicates the absence of the soliton solution ($\tau_\mathrm{p} < 8$).

the NSE soliton. In this case, the duration of such long pulses is approximately equal to τ_p/ω.

It should be noted that solution (44) exists only in the bounded-from-below range $\tau_\mathrm{p}^2 > 8$, which corresponds to the solitons with length exceeding a third of the laser field period (to be more accurate, the limiting duration is equal to $2.31/\omega$ at $\tau_\mathrm{p}^2 = 8$). At $\tau_\mathrm{p}^2 = 8$, the phase plane of Eq. (41) undergoes a bifurcation. One can see this most easily from analyzing the potential at the extremum point ($f = 1/\sqrt{3}$): the potential switches its sign, which corresponds to the jumpwise transition from the soliton solution to the solution with the singularity associated with the formation of the shock wave (Fig. 6). It should be noted that the transition to increasingly shorter solitons is accompanied by the formation of an increasingly stronger soliton phase modulation, which is described by formula (40), similarly to the case of the NSE soliton with nonlinear dispersion.

In contrast with the NSE solitons, the propagation velocity of ultrashort solitons depends on their amplitude, $v = (1 + 1/\tau_\mathrm{p}^2)\,\omega^2/(\sigma + 2X) \propto f_\mathrm{max}^2$. This provides the new channel of the instability of the spatiotemporal solution. Indeed, let the input of the nonlinear medium be fed with an out-of-phase spatiotemporal packet, which is close to the obtained soliton but has slightly different amplitudes in the cores. In this case, there is a spread in the soliton velocities in different cores. Thus, the obtained solution is stable if the transfer length $2\pi/X$ is shorter than the characteristic nonlinear length (the dispersion length $2\omega\tau_\mathrm{p}^2$), i.e., at the strong enough coupling between the adjacent cores [23],

$$X \gg \pi/(\omega\tau_\mathrm{p}^2). \tag{45}$$

The numerical modeling of propagation of ultrashort out-of-phase solitons shows good agreement with this stability estimate. The dashed line in Fig. 7 indicates the boundary (45), and the dots and crosses denote the results of examining the stability numerically.

5. OUT-OF-PHASE SOLUTIONS OF GENERAL FORM

In the previous sections, we have found out-of-phase distributions of the wave field in a fiber with the ring-shaped configuration of the cores. A drawback of this configuration is the technical difficulty of achieving the required sufficiently accurate uniform positioning of the cores along the ring. Moreover, if the number of the cores is great due to the large gap at the center, the diameter of the fiber becomes rather great, which makes it inconvenient for practical use. Therefore, the problem arises to find an out-of-phase distribution of the wave field in fibers with a different configuration of the cores that enables tighter core packing. There are few core lattices that fill the plane tightly: a linear one, a square one, and a hexagonal one. The triangular array is of course not suited for out-of-phase supermodes since the requirement of the field sign reversal in the adjacent cores cannot be fulfilled. In all the above-specified options, there are boundary points that once coupled with a less number of cores than points in the central region. Therefore, it should be expected that the amplitude of the out-of-phase wave field should vary from core to core, which makes it even more difficult to find stable out-of-phase distributions. Let us consider these three options of core configurations in more detail.

5.1. Line of cores

For a start, we confine ourselves to the case of wave beams, for which the dispersion of the medium can be neglected ($\alpha = 0$). Equation (3) for configuration of the cores arranged in a line takes the form

$$i\frac{\partial u_n}{\partial z} = u_{n+1} + u_{n-1} + |u_n|^2 u_n, \quad u_0 = u_{N+1} = 0. \tag{46}$$

In the evolution, Eqs. (46) conserve the total power of the wave beam $P = \sum_{n=1}^{N} |u_n|^2 = \text{const}$.

We seek the solution in the form $u_n(z) = (-1)^n v(n,z)\exp(2iz)$, where $n = 0, \ldots, N+1$ is the coordinate along the core array. We included two "virtual" points $n = 0$ and $n = N+1$ at the boundaries on purpose so that the field at these points vanishes, $v(0,z) = v(N+1,z) = 0$. The use of the dispersion relation $h = -2\cos\varkappa$ of the linearized equation (46) for the processes of the form $\exp(ihz + i\varkappa n)$ allows one to obtain the equation for the complex envelope $v(n,z)$ in the long-wavelength approximation. Assuming that the field envelope $v(n,z)$ is a smooth function ($|\partial v/\partial n| \ll \pi|v|$) and the core number is large ($N \gg 1$), we arrive at the NSE-type equation

$$i\frac{\partial v}{\partial z} = -\frac{\partial^2 v}{\partial n^2} + |v|^2 v. \tag{47}$$

Its distinctive feature is the presence of the minus sign in front of the second derivative. As a result, the focusing nonlinearity of the medium acts as the defocusing one for an out-of-phase distribution of the wave field. This allows one to suggest that there exists a smooth stable distribution of the wave field which does not undergo filamentation instability.

We search for such solution in the form $v = Vf(\varkappa n)\exp(-i\lambda z)$, where V is the amplitude of the wave beam, and λ is the longitudinal wave number. Substituting this expression into Eq. (47), we obtain the equation for the envelope f,

$$\varkappa^2 f'' + \lambda f - V^2 f^3 = 0. \tag{48}$$

This equation has a solution in the form $f(\xi) = \mathrm{sn}(\xi, m)$ with the parameters found from the initial and boundary conditions $f(0) = f[(N+1)\varkappa] = 0$,

$$2m\varkappa^2 = V^2, \quad (N+1)\varkappa = 2K(m), \quad \lambda = (1+m)\varkappa^2. \tag{49}$$

Here, $K(m) = \int_0^{\pi/2} (\sqrt{1 - m\sin^2\varphi})^{-1}\,\mathrm{d}\varphi$ is the complete elliptic integral of the first kind, and the parameter

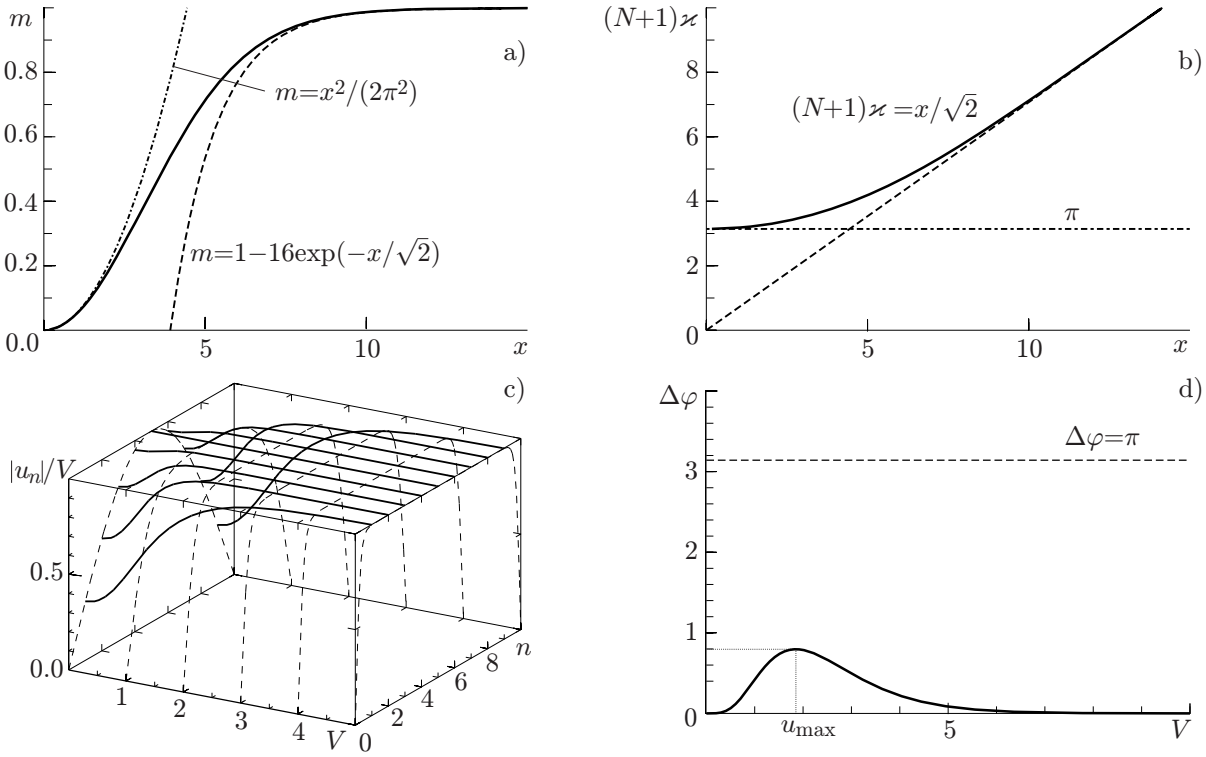

Fig. 8. (*a*) and (*b*) Dependences of m and $\varkappa$ on the dimensionless parameter $x = (N+1)V$ and their approximations (51) and (52). (*c*) Amplitude profile of solution (53) depending on the amplitude V at $N = 9$. (*d*) Maximum phase difference (see formula (54)).

m varies in the range [0,1) and is found from the transcendental equation

$$mK(m)^2 = \frac{1}{8}(N+1)^2 V^2. \tag{50}$$

The graphic solution for the parameter m in Fig. 8 has a step shape with the inflection point at $(N+1)V \approx 4$. The asymptotic solutions of this solution at small and large amplitudes have the form

$$m \approx \begin{cases} (N+1)^2 V^2/(2\pi^2), & (N+1)V \ll 4; \\ 1 - 16\,\exp[-(N+1)\,V/\sqrt{2}], & (N+1)V \gg 4. \end{cases} \tag{51}$$

As seen in Fig. 8, the asymptotic solutions obtained for the parameter m agree well with the graphic solution. Correspondingly, for the transverse wave number $\varkappa$, we get the approximations

$$\varkappa = \frac{2K(m)}{N+1} \approx \begin{cases} \pi/(N+1), & (N+1)V \ll 4; \\ V/\sqrt{2}, & (N+1)V \gg 4. \end{cases} \tag{52}$$

As a result, the stationary solution for the complex envelopes of the wave field have the form

$$u_n = (-1)^n V \exp(i\lambda z)\,\mathrm{sn}(\varkappa n, m) \approx (-1)^n V \exp(i\lambda z) \cdot \begin{cases} \sin[\pi n/(N+1)], & (N+1)V \ll 4; \\ 1, & (N+1)V \gg 4. \end{cases} \tag{53}$$

Thus, in the case of low power, the distribution of the intensity of the wave beam is inhomogeneous in the transverse direction, $|u_n|^2 \propto \sin^2[\pi n/(N+1)]$. At a large power, the field intensity is distributed homogeneously over all the cores, $|u_n|^2 \propto \mathrm{const}$. The forms of the solution at different amplitudes are shown in Fig. 8*c*.

Solution (53) was obtained within the framework of the approximate continuum equation (47). The discreteness present in Eqs. (46) can result in the stability loss of this approximate solution and lead to stochastic dynamics if the difference in the nonlinear phase incursion $\Delta\varphi$ between the adjacent cores over the length of the coupling between them (this length is equal to 1 for Eqs. (46)) exceeds π. In our case, the difference in the phase incursion due to the nonlinearity between the adjacent cores is equal to the difference of the intensities, $\Delta\varphi = \max_n(|u_{n+1}|^2 - |u_n|^2)$. The value of $\Delta\varphi$ can become noticeably greater only for the field amplitudes $u_n \sim V > 1$. Therefore, it is sufficient to evaluate the phase difference in the region $(N+1)V \gg 4$. Then we can expand the found solution (53) near the boundary (where the gradients are the maximum) and obtain

$$\Delta\varphi \;\le\; |u_2|^2 - |u_1|^2 \;=\; V^2\big[\,\mathrm{sn}(2\varkappa,\mu)^2 - \mathrm{sn}(\varkappa,\mu)^2\big] \;\approx\; V^2\left[\tan^2(\sqrt{2}V) - \tan^2(V/\sqrt{2})\right] \;<\; 0.8. \quad (54)$$

Here, we used the approximations $\mathrm{sn}(x, \mu \to 1) \approx \tan(x)$ and $\varkappa \approx V/\sqrt{2}$ at $(N+1)V \gg 4$ (Fig. 8*d*). The maximum of the phase difference $\Delta\varphi \approx 0.8 \ll \pi$ corresponds to the field amplitude $V = u_* \approx 1.852$. Thus, it is impossible to reach the threshold of stochastic dynamics on the solution (53). The reason for this is as follows. Despite the great values of $\varkappa$ at $V \gg 4/(N+1)$, the entire variation in the wave field distribution $a(n)$ from 0 to V fits the virtual region $0 \le n < 1$ and $N > n \ge N+1$, whereas there are no sharp gradients of the wave field in the physically correct region $1 \le n \le N$.

Knowing the solution (53) for the complex envelopes allows one to predict the nonlinear dynamics of the wave field in an active fiber if the growth scale of the power and, correspondingly, the maximum amplitude $u_{\max}$ exceeds the transfer length significantly (e.g., if the gain $\gamma \ll 1$ in an active medium). As the wave beam power increases exponentially, the adiabatically smooth flattening of the amplitudes in all the cores is expected at $u_{\max} > u_{\mathrm{th}} \equiv 4/(N+1)$. The adiabaticity holds, if the gain is smaller than the difference of the propagation constant between the antiphase supermode and other supermodes of the fiber. The propagation constants of Eqs. (46) are equal to $h_n = 2\cos[\pi m/(N+1)]$ at $|u_n|^2 \ll 1$. The smallest of them, $h_N = 2\cos[\pi N/(N+1)]$, corresponds to the found out-of-phase distribution (53). Then the adiabaticity condition of the amplification process is

$$\gamma \ll 4\sin\frac{3\pi/2}{N+1}\sin\frac{\pi/2}{N+1} \approx \frac{3\pi^2}{(N+1)^2} < 1. \quad (55)$$

It is seen from this expression that the limiting gain at which other supermodes are not excited decreases rather fast with the number of cores.

The out-of-phase solution (53) can be generalized for the case of a lattice of the dimensions $2 \times N$, such lattice described by the equations

$$\begin{aligned} i\frac{\partial u_{1,n}}{\partial z} &= u_{1,n+1} + u_{1,n-1} + u_{2,n} + \mu(u_{2,n-1} + u_{2,n+1}) + |u_{1,n}|^2 u_{1,n}. \\ i\frac{\partial u_{2,n}}{\partial z} &= u_{2,n+1} + u_{2,n-1} + u_{1,n} + \mu(u_{1,n-1} + u_{1,n+1}) + |u_{2,n}|^2 u_{2,n}. \end{aligned} \quad (56)$$

In these equations, weak diagonal coupling $\mu \ll 1$ between the cores, which exists in actual fibers, is introduced. The substitution $u_{k,n} = (-1)^k g_n \exp(-iz)$ $(k = 1, 2)$ yields the equation

$$i\frac{\partial g_n}{\partial z} + (1-\mu)(g_{n-1} + g_{n+1}) + |g_n|^2 g_n = 0, \quad (57)$$

which coincides with Eq. (46) except for the intercore coupling coefficient being equal to $1 - \mu$ instead of 1.

5.2. Square configuration

The transition from a fiber with the cores arranged in a line to a fiber with a rectangular array of the cores presents certain difficulties when analytical solutions are derived since they cannot be written in terms of the simplest special functions. A special case is the square matrix of the cores, where the field can be described by a small number of variables thanks to the symmetry of the problem.

We again confine ourselves to the case of wave beams with neglectable dispersion, $\alpha = 0$. Equation (3) for the core configuration in the form of a square matrix takes the form

$$i\frac{\partial u_{n,m}}{\partial z} = u_{n+1,m} + u_{n-1,m} + u_{n,m+1} + u_{n,m-1} + |u_{n,m}|^2 u_{n,m},$$
$$u_{n,0} = u_{n,N+1} = u_{0,m} = u_{N+1,m} = 0. \tag{58}$$

In the evolution, Eqs. (58) conserve the total power $P = \sum |u_{n,m}|^2 = \text{const}$.

By analogy with the case of the core line, we seek the out-of-phase solution in the form $u_{n,m}(z) = (-1)^{n+m} v(n,m,z) \exp(4iz)$, where $\{m,n\} = 0,\ldots,N+1$ are the coordinates along the array. We included the virtual points $\{m,n\} = 0$ and $N+1$ on the boundaries on purpose so that the field vanishes at them, $v(n,0,z) = v(n,N+1,z) = v(0,m,z) = v(N+1,m,z) = 0$. The use of the dispersion relation $h = -2(\cos\varkappa_1 + \cos\varkappa_2)$ of linearized equation (58) for the processes having the form $\exp(ihz + i\varkappa_1 n + i\varkappa_2 m)$ allows one to obtain the equation for the complex envelope $v(n,m,z)$ in the long-wavelength approximation. Assuming that the envelope is a smooth function ($\{|\partial v/\partial n|, |\partial v/\partial m|\} \ll \pi|v|$) and the number of cores is large ($N \gg 1$), we arrive at the NSE-type equation

$$i\frac{\partial v}{\partial z} = -\frac{\partial^2 v}{\partial n^2} - \frac{\partial^2 v}{\partial m^2} + |v|^2 v. \tag{59}$$

Note that the sign of the nonlinearity remains the same, i.e., it is focusing. However, the sign of the diffraction terms has changed, since the out-of-phase distribution is located at the boundary of the Brillouin zone. As a result, the character of Eq. (59) has become defocusing. This allows one to suggest that there exists a smooth stable out-of-phase distribution of the wave field.

One can solve Eq. (59) easily in the limit of small amplitudes where the influence of the medium nonlinearity can be neglected,

$$v(n,m) \approx G \sin\frac{\pi n}{N+1} \sin\frac{\pi m}{N+1}, \quad |G|^2 \equiv \frac{4P}{(N+1)^2} \ll 1. \tag{60}$$

This solution corresponds to the well-known lowest mode of the rectangular waveguide. In the case of large amplitudes, the influence of the nonlinearity is dominant, and the solution should tend to homogeneous distribution (similarly to Eq. (53)):

$$v(n,m) \approx G, \quad |G|^2 \equiv P/N^2 \gg 1. \tag{61}$$

In the case of large-size square matrices, the filamentation instability along the diagonal directions becomes possible, where the field in the cores is in phase. To describe this possibility, one should take into account the minor diagonal coupling $\zeta \ll 1$ in Eqs. (58):

$$i\frac{\partial u_{n,m}}{\partial z} + u_{n+1,m} + u_{n-1,m} + u_{n,m+1} + u_{n,m-1} + |u_{n,m}|^2 u_{n,m}$$
$$+ \zeta\left(u_{n+1,m+1} + u_{n-1,m+1} + u_{n+1,m-1} + u_{n-1,m-1}\right) = 0. \tag{62}$$

The propagation of high-power laser radiation with the out-of-phase field distribution leads to the flattening

of the amplitudes, see Eq. (61). Then the unperturbed solution with the amplitude u_0 can be expressed as

$$u^{(\mathrm{s})}_{n,m} = u_0(-1)^{n+m}\exp(ihz), \quad h = 4(1-\zeta) - u_0^2. \tag{63}$$

Let us examine this solution in regard to the filamentation instability. Substituting the wave field in the form of solution (63) with the perturbations included, $u_{n,m} = u_0\big[(-1)^{n+m} + \delta\exp(i\varkappa_1 m + i\varkappa_2 n)\big]\exp(ihz)$, into Eq. (62) and linearizing it with respect to the minor perturbations $\delta \ll 1$, we obtain

$$i\frac{\partial\delta}{\partial z} = h\delta + u_0^2(2\delta+\delta^*) + 2\left[\cos\varkappa_1 + \cos\varkappa_2 + 2\zeta\cos(\varkappa_1)\cos\varkappa_2\right]\delta. \tag{64}$$

This equation has solutions in the form $\{\delta,\ \delta^*\} \propto \exp(\Gamma z)$ with

$$\Gamma^2 = u_0^2 - (\mathcal{K} + u_0^2)^2, \quad \mathcal{K} = 2\cos\varkappa_1 + 2\cos\varkappa_2 + 4\zeta\cos(\varkappa_1)\cos\varkappa_2. \tag{65}$$

The real part of Γ becomes positive at $\mathcal{K} < 0$, i.e., only at $\zeta \geq 1/2$. This corresponds to a rather great coupling coefficient that violates the used approximation of weakly coupled cores. Therefore, the found out-of-phase distribution of the wave field is not prone to the filamentation instability.

It is difficult to find the exact analytical solution in the square configuration of the cores in the general case. Therefore, the solution of Eqs. (58) for the out-of-phase distribution of the intense wave field in the square core matrix ($N \times N$) can be obtained in two ways: by applying the variational approach or by analyzing the equations for a rather small N with account of the problem symmetry. Let us consider these ways in depth.

It seems reasonable to try first the variational approach in the case of the linear arrangement of cores with known solution (Sec. 6.4). The main difficulty with using the variational approximation is the complicated spatial structure of the out-of-phase distribution. The matter is that the presence of the Jacobian elliptic sine (as in solution (53)) makes the integrals hard to evaluate and bulky, while the use of a series of common sine functions yields the results converging slowly to the exact solution. Among the simple-to-integrate dependences, the power-law distribution over the transverse coordinate

$$u_n = \sqrt{\frac{P(a+1)(2a+1)}{2Na^2}}(1-|\xi|^a)\exp(ib\,|\xi|^a + i\varphi), \quad \xi = \frac{2n}{N+1} - 1. \tag{66}$$

allows one to achieve good agreement with solution (53). Here, $a_{\min} = (1+\sqrt{6})/2 \approx 1.72$ corresponds to the limiting case of the linear problem ($m = 0$ in solution (53)). We also took into account that the inhomogeneous phase incursion across the beam ($\propto b|\xi|^a$) is proportional to the inhomogeneity of the wave field amplitude. Distribution (66) conserves the total beam power $P = (N/2)\int_{-1}^{1}|u_n|^2\,\mathrm{d}\xi \approx \sum|u_n|^2$.

Substituting Eqs. (66) into Eq. (47), we find the reduced action

$$S = \int \frac{P}{N}\left[\frac{(4a^2b^2+24a^2-14a+2)(a+1)(2a+1)}{(2a-1)(3a-1)(4a-1)N^2} + \frac{3P}{N}\frac{(a+1)(2a+1)}{(3a+1)(4a+1)} + \frac{11a^2+12a+3}{(a+1)(2a+1)(3a+1)^2}b\frac{\mathrm{d}a}{\mathrm{d}z} - \frac{1}{3a+1}\frac{\mathrm{d}b}{\mathrm{d}z} - \frac{\mathrm{d}\varphi}{\mathrm{d}z}\right]\mathrm{d}z, \tag{67}$$

and taking the variational derivative of this action, we obtain the equations for the parameters a and b. These equations have an equilibrium point (of the center type) at

$$P = \frac{(3a+1)^2(4a+1)^2(4a^2-4a-5)}{3N\,(2a-1)^2(11a^2+10a+2)}, \quad b = 0, \tag{68}$$

which corresponds to a stable out-of-phase distribution. To compare the found approximate solution and the

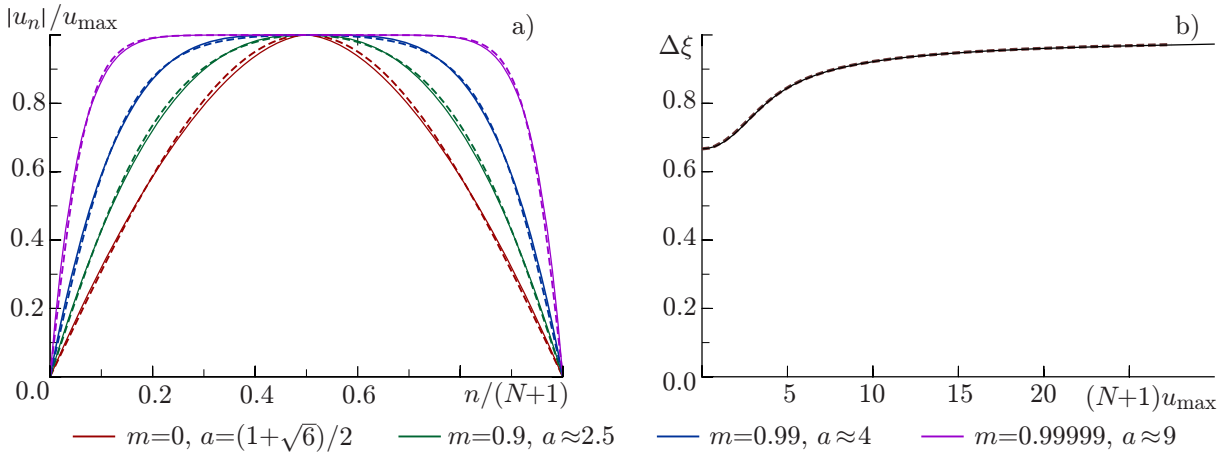

Fig. 9. (*a*) Transverse structure of the solutions at various values of the parameters: the dashed and solid lines correspond to the exact and approximate solutions given by (Eqs. (53) and (66), respectively). (*b*) Half-width $\Delta\xi$ as a function of the maximum amplitude $u_{\max}$ in the exact and approximate solutions (the dashed and solid lines, respectively).

exact solution (53), we plot the dependence of the maximum amplitude $u_{\max}$ on the amplitude full width $\Delta\xi$ at half-maximum,

$$\Delta\xi = \frac{1}{\sqrt[a]{2}} = 1 - \frac{F(\pi/6, m)}{K(m)} \approx 1 - \frac{\ln 3}{\ln 8 - \ln(1-m)}, \tag{69}$$

where $F(\phi, m)$ is the incomplete elliptic integral of the first kind. Figure 9*b* shows very good agreement between the exact solution obtained from the variational approach and the approximate solution. This allows the hope of the same good accuracy of the approximate out-of-phase solution in the square configuration.

The generalization of the variational approach (66) to the case of the square configuration of the cores looks rather simple. We search for the distribution with the power-law dependence on the both coordinates:

$$u_{n,m} = \sqrt{P}\frac{(a+1)(2a+1)}{2Na^2}(1-|\xi|^a)(1-|\zeta|^a)\exp[ib(|\xi|^a+|\zeta|^a)+i\varphi], \quad \xi = \frac{2n}{N+1}-1, \quad \zeta = \frac{2m}{N+1}-1. \tag{70}$$

Once more, $a_{\min} = (1+\sqrt{6})/2 \approx 1.72$ corresponds to the limiting case of the linear problem. We also again took into account that the inhomogeneous phase incursion across the beam ($\propto b|\xi|^a + b|\zeta|^a$) is proportional to the inhomogeneity of the wave field amplitude. The distribution (70) conserves the total beam power $P = (2/N)\iint |u_{n,m}|^2\,\mathrm{d}\xi\,\mathrm{d}\zeta \approx \sum |u_{n,m}|^2$.

Substituting Eqs. (70) into Eq. (59), we find the reduced action

$$S = \int \frac{P}{N^2}\left[\frac{(8a^2b^2+48a^2-28a+4)(a+1)(2a+1)}{(2a-1)(3a-1)(4a-1)N^2} + \frac{18P}{N^2}\frac{(a+1)^2(2a+1)^2}{(3a+1)^2(4a+1)^2} + \frac{22a^2+24a+6}{(a+1)(2a+1)(3a+1)^2}b\frac{\mathrm{d}a}{\mathrm{d}z} - \frac{2}{3a+1}\frac{\mathrm{d}b}{\mathrm{d}z} - \frac{\mathrm{d}\varphi}{\mathrm{d}z}\right]\mathrm{d}z, \tag{71}$$

and taking the variational derivative of this action, we obtain the equations for the parameters a and b with the equilibrium point

$$P = \frac{(3a+1)^3(4a+1)^3(4a^2-4a-5)}{18\,(a+1)(2a+1)(2a-1)^2(11a^2+10a+2)}, \quad b = 0 \tag{72}$$

corresponding to the stable out-of-phase distribution.

We compare this solution with the exact solution for a square 5×5 matrix. In this case, the out-of-

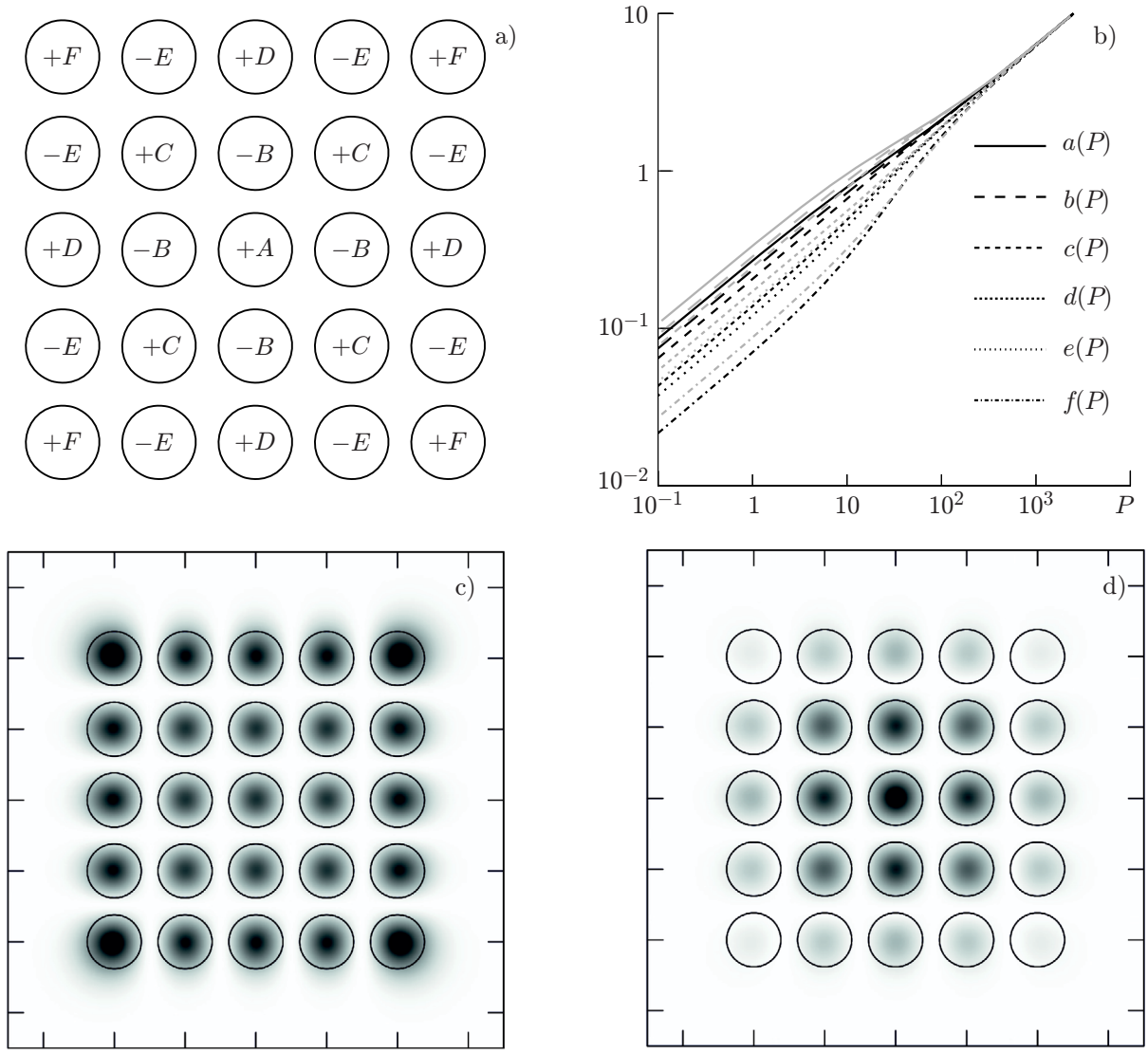

Fig. 10. (*a*) Transverse structure of the out-of-phase supermode in a fiber containing the 5×5 core array. (*b*) Amplitudes in the cores as functions of the total power P in the exact and approximate solutions (black and gray lines, respectively). Panels (*c*) and (*d*) show the typical distribution of the intensity in the supermode at high and low powers, respectively. The color saturation indicates the field intensity from zero (white) to the maximum (black).

phase stationary distribution of the wave field can be described by six independent variables by virtue of the symmetry of the square matrix (Fig. 10*a*). This reduces the equation set (58) to

$$i\dot{A} = -4B + |A|^2 A, \quad i\dot{B} = -A - 2C - D + |B|^2 B, \quad i\dot{C} = -2B - 2E + |C|^2 C, \tag{73a}$$

$$i\dot{D} = -B - 2E + |D|^2 D, \quad i\dot{E} = -C - D - F + |E|^2 E, \quad i\dot{F} = -2E + |F|^2 F. \tag{73b}$$

As the final equation, one should include the conservation law for the total power $P = |A|^2 + 4|B|^2 + 4|C|^2 + 4|D|^2 + 8|E|^2 + 4|F|^2$.

Since we are interested in stationary solutions, we replace

$$\{A, B, C, D, E, F\} = \{a, b, c, d, e, f\} \exp(i\lambda z)$$

and reduce Eqs. (73) to a set of seven algebraic equations depending on the single parameter P. At low

amplitudes, one can neglect the nonlinearity and obtain the relation between the amplitudes and the power (see Fig. 10*d*):

$$\frac{b}{a}\approx\frac{\sqrt{3}}{2}+\frac{7}{4}\frac{P}{12^2},\quad \frac{c}{a}\approx\frac{3}{4}+\frac{13\sqrt{3}}{8}\frac{P}{12^2},\quad \frac{d}{a}\approx\frac{1}{2}+\frac{7\sqrt{3}}{4}\frac{P}{12^2},\quad \frac{e}{a}\approx\frac{\sqrt{3}}{4}+\frac{25}{8}\frac{P}{12^2},$$
$$\frac{f}{a}\approx\frac{1}{4}+\frac{11\sqrt{3}}{8}\frac{P}{12^2},\ a\approx\frac{\sqrt{P}}{3}-\frac{13\,P^{3/2}}{864\sqrt{3}}\ll 1. \tag{74}$$

The obtained values coincide with solution (60) found in the long-wavelength limit. At large amplitudes, one can neglect the linear terms and obtain the solution (see Fig. 10*c*)

$$\frac{b}{a}\approx 1-\frac{5^4}{4P^2},\quad \frac{c}{a}\approx 1-\frac{5^4}{2P^2},\quad \frac{d}{a}\approx\frac{e}{a}\approx 1-\frac{5^2}{4P},\quad \frac{f}{a}\approx 1-\frac{5^2}{P},\quad a\approx\frac{\sqrt{P}}{5}+\frac{2}{\sqrt{P}}\gg 1 \tag{75}$$

with the homogeneous intensity distribution over the cores, similar to solution (53) in the line of cores. The numerical solutions of the equations are shown in black in Fig. 10*b*. Similar dependences obtained within the framework of the approximate solution (70), (72), are shown in gray in Fig. 10*b*, where their good agreement with the exact solution at $N = 5$ is evident. A slight difference at low powers is related to the noticeable discreteness of the square 5×5 configuration.

5.3. Hexagonal configuration

Consider the wave field distributions in another version of the core configuration with arrangement as a set of seven rings (central ring and six more rings at each face) [20] shown in Fig. 11*a*. The wave field dynamics in such a system is rather complex: The most typical cases are quasirandom beat waves and field concentration in a single light guide due to an analog of the filamentation instability. However, a stable spatial distribution for the out-of-phase supermode is present in the system [20]. The main difference between the sought-for mode and the out-of-phase supermode on a single ring (see Sec. 4) consists in the possibility of radial oscillations between the rings of the radii r, $2r$, and $\sqrt{7}r$. Therefore, the field amplitudes can be different at the three above-specified radii similarly to the cases of a line or a square matrix of the cores.

We assume that the field amplitude is the same at each of the radii and denote the respective field amplitudes as a, b, and c (Fig. 11*a*). The equations for the complex envelopes a, b, and c have the form [20]

$$i\frac{\partial a}{\partial z}=-2a-b+|a|^2a,\quad i\frac{\partial b}{\partial z}=-a-2c+|b|^2b,\quad i\frac{\partial c}{\partial z}=-b-c+|c|^2c. \tag{76}$$

These equations conserve the total beam power $P=6|a|^2+6|b|^2+12|c|^2$. This allows one to reduce the dimensionality of the problem and search for the solution of Eqs. (76) in the form [20]

$$a=\sqrt{\frac{PA}{6}}\exp[i(\theta+\zeta)],\quad b=\sqrt{\frac{PB}{6}}\exp[i(\phi+\zeta)],\quad c=\sqrt{\frac{P}{12}(1-A-B)}\exp(i\zeta).$$

Here, A is the fraction of the radiation power fraction in the central ring, and B is the power fraction in the middle ring. For the evolution of the wave beam parameters $\{A, B, \phi, \zeta, \theta\}$ along the propagation path, we obtain a set of ordinary differential equations

$$\frac{\mathrm{d}A}{\mathrm{d}z}=-\frac{\partial\mathcal{H}}{\partial\theta},\qquad \frac{\mathrm{d}B}{\mathrm{d}z}=-\frac{\partial\mathcal{H}}{\partial\phi},\qquad \frac{\mathrm{d}\phi}{\mathrm{d}z}=\frac{\partial\mathcal{H}}{\partial A},\qquad \frac{\mathrm{d}\theta}{\mathrm{d}z}=\frac{\partial\mathcal{H}}{\partial B},$$
$$\mathcal{H}=\frac{P}{24}\left[3B^2+2AB+3A^2-2(A+B)\right]+B-A-2\sqrt{AB}\cos(\phi-\theta)-2\sqrt{2B(1-B-A)}\cos\phi. \tag{77}$$

The equation for the evolution of the common phase ζ is detached from the equations for the dynamics of

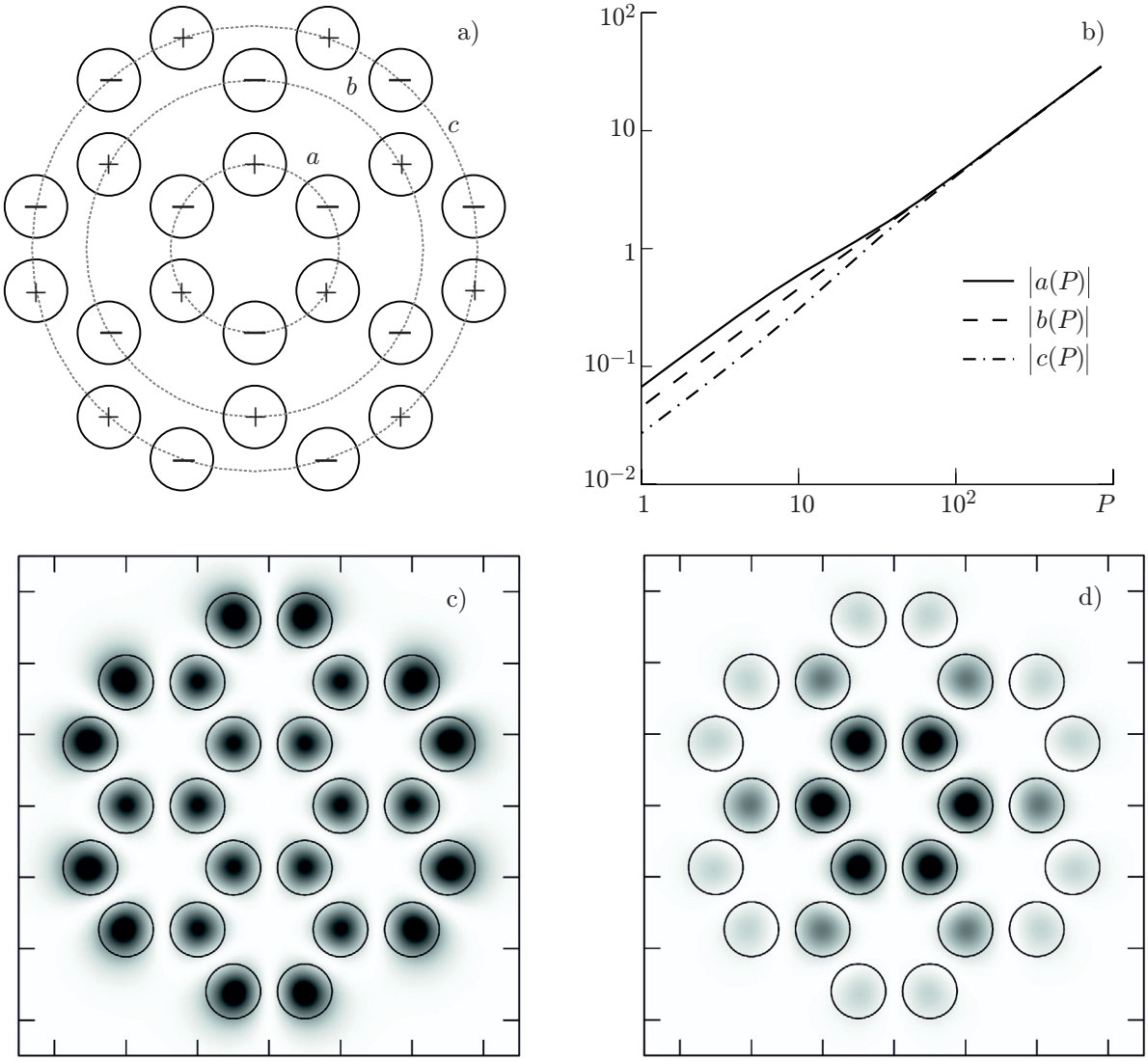

Fig. 11. (*a*) Transverse structure of the out-of-phase supermode in a fiber containing 24 cores. (*b*) Amplitudes in the cores as functions of the total power P. Panels (*c*) and (*d*) show the typical distribution of the intensity in the supermode at high and low powers, respectively. The color saturation indicates the field intensity from zero (white) to the maximum (black).

the rest of parameters of the wave beam. An integral of these equation is the hamiltonian $\mathcal{H}$.

The analysis of the obtained four-dimensional set (77) is complicated. However, from the viewpoint of the coherent radiation propagation in the system under consideration, only stationary distributions (supermodes) are of interest. Let us find them and examine their stability. The equilibrium points are found at $\theta = 0, \pi$, and $\phi = 0, \pi$. In this case, only $\theta = 0$, $\phi = 0$ is an absolutely stable stationary point, since all the second derivatives of the hamiltonian are always positive there. Substituting $\theta = 0$ and $\phi = 0$ to Eqs. (77), we arrive at two algebraic nonlinear equations for the values A and B of the stable mode [20]:

$$\sqrt{\frac{A}{B}} - \frac{\sqrt{2}(2B + A - 1)}{\sqrt{B(1 - B - A)}} - 1 = \frac{P}{12}(3B + A - 1), \tag{78a}$$

$$\sqrt{\frac{B}{A}} - \frac{\sqrt{2B}}{\sqrt{1 - B - A}} + 1 = \frac{P}{12}(B + 3A - 1). \tag{78b}$$

The analytical solution of this set of equations is too complicated. It is easy to find only the asymptotics at high powers P,

$$A \approx \frac{1}{4} + \frac{3}{P}, \quad B \approx \frac{1}{4} + \frac{3}{P+48}, \quad \frac{|c|^2}{P} \approx \frac{1}{4} - \frac{3}{P+24}; \tag{79}$$

this asymptotics corresponds to the quasihomogeneous distribution of the intensity over all the light guides. The form of the nonlinear supermode at the arbitrary power P is shown in Fig. 11*b*. It is evident from the figure that the field in the mode obtained is concentrated mainly in the internal cores ($a > b > c$, Fig. 11*d*) at a low total power P, and the mode intensity is distributed almost uniformly over all the cores ($a \approx b \approx c$, Fig. 11*c*) at a high power level ($P \geq 100$). In the latter case, the maximally transported power is $\mathcal{P} \lesssim 24\mathcal{P}_{\rm cr}$ [20].

Knowing the equilibrium states (78) allows one to predict the nonlinear dynamics of the wave field in the active fiber when the power increases smoothly due to small gain at $\gamma \ll 1$, i.e., amplification is weak on the scale of the transfer length. As the wave beam power increases exponentially, adiabatically smooth flattening of the amplitudes over all the cores has to be expected [20].

6. RING–CENTER CONFIGURATION

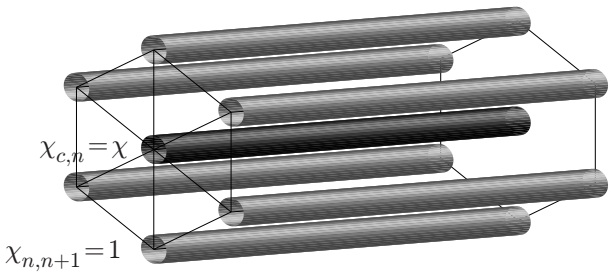

Fig. 12. Structure of the fiber with the cores arranged in the ring around the central core.

It should be noted that an analog of the discrete collapse considered in Sec. 3.1 can also appear in fibers containing not-too-many cores. For example, in the ring configuration of the light guides all the linear supermodes, but the antiphase one, are unstable, with the in-phase supermode of $m = 0$ (Sec. 4.1) having the largest instability increment. The instability leads to a sharp increase in the amplitude in one of the cores; such effect alone can be used in various applications including radiation collection, nonlinear filtration, pulse compression, etc. To make the instability more controllable, one can introduce the central core coupled with rest of the cores in the ring (Fig. 12). One may expect that the radiation should be trapped in this very core [35, 36]. Let us find the nonlinear in-phase supermode to verify this statement.

Equation (3) for the in-phase mode in such a core configuration takes the form [35]

$$\begin{aligned} i\frac{\partial a}{\partial z} &= 2N\chi f + |a|^2 a + \alpha\frac{\partial^2 a}{\partial \tau^2}, \\ i\frac{\partial f}{\partial z} &= \chi a + 2f + |f|^2 f + \alpha\frac{\partial^2 f}{\partial \tau^2}. \end{aligned} \tag{80}$$

Here, a and f are the amplitude in the central core and on the ring, respectively, χ is the couping coefficient with the central core, and the coupling coefficients between the cores along the ring were set equal to unity without loss of generality.

6.1. In-phase wave beams

We start analyzing Eqs. (80) with the case of the beam problem ($\alpha = 0$). The conservation law of the total wave beam power $P = |a|^2 + 2N|f|^2 = \text{const}$ allows one to reduce the number of variables and search for the solution of Eqs. (80) in the form $a = \sqrt{PA}\exp[i\,(\phi+\theta)]$, $f = \sqrt{(1-A)P/2N}\exp(i\phi)$, where A is the fraction of the power in the central core and θ is the phase difference between the amplitude on the ring and at the center. The evolution of the wave beam parameters satisfies the following set of ordinary differential

equations [37]:

$$\frac{\mathrm{d}A}{\mathrm{d}z} = -2\chi\sqrt{2N}\sqrt{A-A^2}\sin\theta, \tag{81a}$$

$$\frac{\mathrm{d}\theta}{\mathrm{d}z} = \sqrt{2N}\chi\frac{2A-1}{\sqrt{A-A^2}}\cos\theta - \frac{(2N+1)PA}{2N} + \frac{P}{2N} + 2. \tag{81b}$$

The equation for the evolution of the phase ϕ is detached from the equations for the dynamics of the rest of the wave-field parameters $\{A, \theta\}$. The two other equations (81a) and (81b) have the integral of motion [37]

$$H = 2P\chi\sqrt{2NA(1-A)}\cos\theta - 2PA + \frac{P^2}{4N}\left[(A-1)^2 + 2NA^2\right], \tag{82}$$

allowing a solution by quadrature of Eqs. (81).

Let us analyze the possible types of solutions of Eqs. (81) on the phase plane (Fig. 13), whose structure depends significantly on the wave beam power P. The right-hand part of Eq. (81a) vanishes at the straight lines $A = 0$ and $A = 1$ corresponding to two distributed saddle-type equilibrium states, whose positions are independent of the input power. These lines are degenerate unstable one-dimensional manifolds corresponding to the field localization either in the central core only (at $A = 1$) or in the ring only (at $A = 0$).

The phase plane in the case of low input power P is shown in Fig. 13*a*. It is apparent that Eqs. (81) have four equilibrium states: two distributed saddle-type equilibrium states ($A = 0$ and $A = 1$) and two centers. At low power ($P \to 0$), these two roots A_{I} and A_{II} approach the values [37]

$$A_{\mathrm{I}}^0 = \frac{1}{2} - \frac{1}{2\sqrt{2N\chi^2+1}}, \quad A_{\mathrm{II}}^\pi = \frac{1}{2} + \frac{1}{2\sqrt{2N\chi^2+1}}, \tag{83}$$

which are equal to the eigenvectors of the normal supermodes in the linear problem.

As the wave beam power increases (Figs. 13*b* and 13*c*), the positions of the centers changes. The center at $\theta = 0$ shifts upward whereas the one at $\theta = \pi$ moves downward. The motions outside of the equilibrium states describe the sequential transfer of energy from the central core (a decrease in A) to the ring of the multicore light guide and back. As the power increases up to the level

$$P_* \approx 6\chi\sqrt{3}N^2 - 6N - \frac{2+\chi^2+2\sqrt{3}\chi}{2\sqrt{3}\chi}, \tag{84}$$

a bifurcation occurs, and a new pair of the equilibrium states appears, those of the center and saddle types (Fig. 13*e*, branches II and IV). As the power increases further, the position of the newly-born center-type equilibrium state shifts toward small values $A \to 0$. At $P > P_*$, the fraction of the transported energy decreases, and solutions with weakly changing amplitudes appear (the centers near the maximum and minimum amplitudes). This regime corresponds to the field trapped in the central core or in the ring only [37].

Analysis of the stability with respect to azimuthal perturbations shows that branch I is stable at all values of the power. Branch II is stable only at low power values, $P \lesssim \pi$. Branches III and IV are always unstable. Thus, isotropic distributions cannot be used to transport wave beams with powers exceeding the critical one for self-focusing in a multicore fiber. However, the presence of nonlinear beating in the transitional region $P < 10$ allows one to use them for nonlinear separation of the desired signal and the low-amplitude noise.

6.2. Self-compression during trapping in the center

The soliton dynamics of the in-phase distribution of the wave field over the cores has its own interesting features. In this section, we take into account the influence of the abnormal medium dispersion ($\alpha > 0$) in

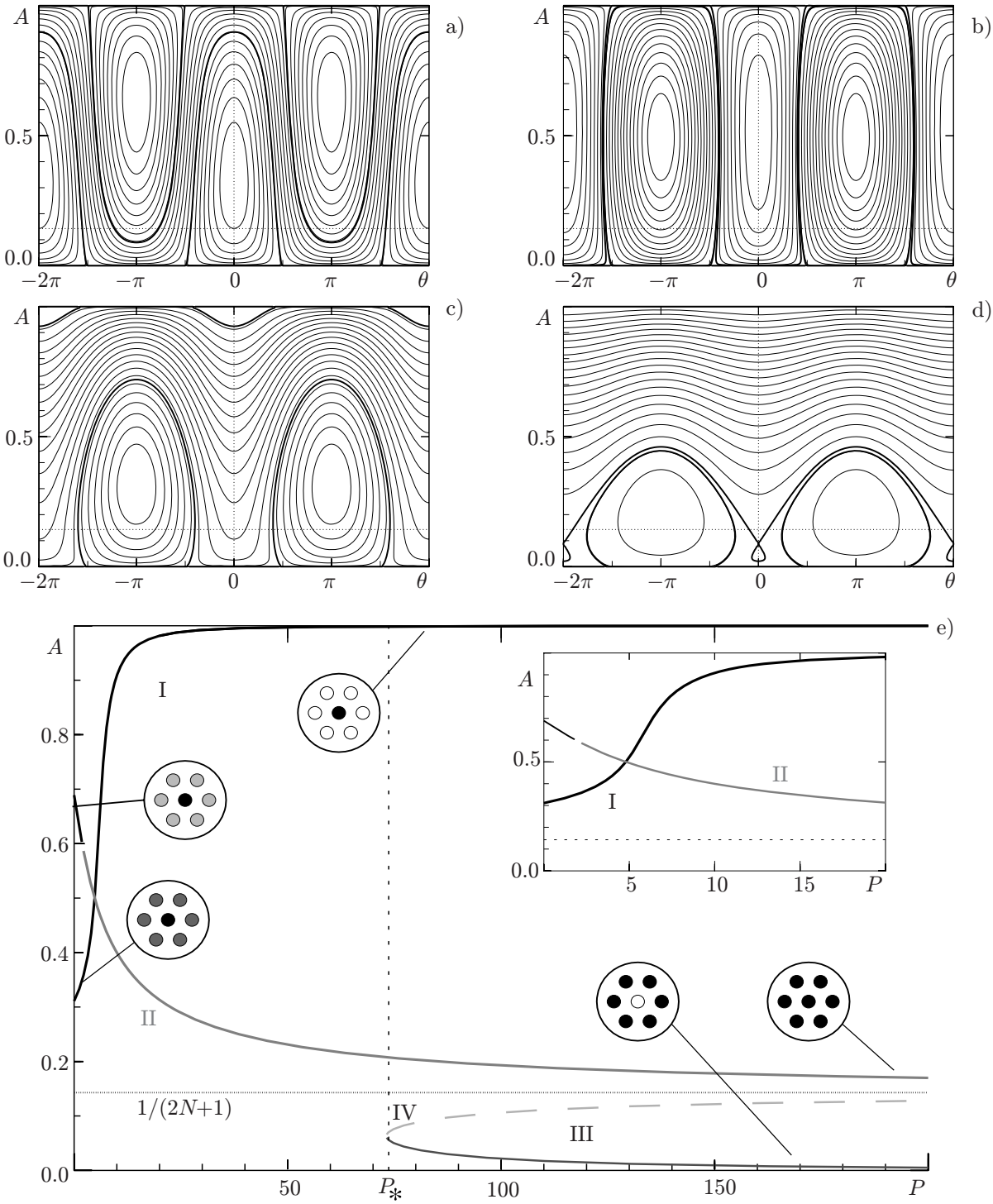

Fig. 13. Phase plane of Eqs. (81) for the case $N = 3$, $\chi = 1$ at different values of the power: $P = 1, 5, 20$, and 80 (*a*, *b*, *c*, and *d*, respectively). The solid lines mark the separatrices. The dotted line $A = 1/(2N + 1)$ corresponds to the homogeneous distribution. (*e*) Equilibrium states of the system as functions of the power P. The heavy black lines refer to the distributions stable with respect to azimuthal perturbations. The round insets present the respective structures of the solutions.

Eqs. (80) and demonstrate the possibility of coherent summation and self-compression of laser pulses in such fibers [35, 36].

The search for exact soliton solutions of Eqs. (80) appears to be complicated. We use the variational

approach to find the approximate quasisoliton solution using the conservation law for the total energy $W = \int(|a|^2 + 2N|f|^2)\,\mathrm{d}\tau$ and having the following form:

$$a = \sqrt{\frac{WA}{2\tau_\mathrm{p}}}\frac{\exp[i(\phi+\theta+\sigma\tau^2)]}{\cosh(\tau/\tau_\mathrm{p})}, \quad f = \sqrt{\frac{W(1-A)}{4N\tau_\mathrm{p}}}\frac{\exp[i(\phi+\sigma\tau^2)}{\cosh(\tau/\tau_\mathrm{p})}. \tag{85}$$

Here, A is the energy fraction in the soliton propagating in the central core, τ_p is the soliton duration, σ is the parameter of the quadratic phase modulation in time (chirp parameter), and θ is the relative difference of the field phases between the central core and the ring.

Substituting the fields in the form (85) into the action for Eqs. (80) and integrating with respect to the variable τ, we obtain a set of ordinary differential equations for evolutions of the wave-packet parameters [35],

$$\frac{\mathrm{d}A}{\mathrm{d}z} = -2\chi\sqrt{2N}\sqrt{A-A^2}\sin\theta, \tag{86a}$$

$$\frac{\mathrm{d}\theta}{\mathrm{d}z} = \chi\sqrt{2N}\frac{2A-1}{\sqrt{A-A^2}}\cos\theta - W\frac{2NA+A-1}{6N\tau_\mathrm{p}} + 2, \tag{86b}$$

$$\frac{\mathrm{d}\tau_\mathrm{p}}{\mathrm{d}z} = -4\sigma\tau_\mathrm{p}, \quad \frac{\mathrm{d}\sigma}{\mathrm{d}z} = 4\sigma^2 + \frac{1}{\pi^2\tau_\mathrm{p}^3}\left[\frac{2NA^2+(A-1)^2}{2N}W - \frac{4}{\tau_\mathrm{p}}\right]. \tag{87}$$

Equations (87) have an equilibrium point [35]

$$\tau_\mathrm{p}^\mathrm{sol} = \frac{4}{W}\frac{1}{A^2+(1-A)^2/2N}, \quad \sigma_\mathrm{sol} = 0 \tag{88}$$

corresponding to the propagation of the soliton-like laser pulse. The oscillations near this center-type equilibrium are similar to the oscillations of a quasisoliton pulse the duration in the NSE.

Same as in the case of the beam problem (Sec. 6.1), the system of equations (86) has four equilibrium states (Fig. 14*a*) at a low total energy $W \ll 1$: two distributed saddle-type equilibrium states ($A = 0$ and $A = 1$) and two centers (83). As the energy of the wave packet increases, the positions of the centers shift: the center at $\theta_\mathrm{sol} = 0$ moves upward (branch I in Fig. 14*d*), and the center at $\theta_\mathrm{sol} = \pi$ moves downward (branch II). The main type of the motion consists in sequential transfer of the energy from the central core (decreasing A) to the ring and back.

As the energy W increases up to the level

$$W_\mathrm{cr} \simeq \frac{8\sqrt{3}}{\sqrt{1-1/(2N)^2}} \approx 8\sqrt{3} \approx 13.86, \tag{89}$$

a bifurcation occurs, and a new pair of the equilibrium states appears: one being of the center type and the other being of the saddle type (Fig. 14*c*). It is important to emphasize that the critical energy does not depend on the coupling coefficient with the central core and depends weakly on the number of the light guides $N \gg 1$. As the energy increases further, the second bifurcation happens, which is related to the merging of the bottom center with the newly-born saddle. The newly-born top center approaches the axis $A \approx 1$ as energy grows. It should be noted that these two bifurcations lead to the hysteresis on curve I. The energy range where the hysteresis takes place is rather narrow; therefore, there is a jumpwise change in A with a small change in W. The position of the hysteresis found is marked on branch I by a vertical dashed line. Finally, at

$$W = W_* \approx 12\sqrt[4]{3}\sqrt{\chi}N^{3/2} + 6\sqrt[4]{3}(5\chi - 6\sqrt{3})\sqrt{\chi N}, \tag{90}$$

the third bifurcation takes place where two equilibrium states are born: a center (branch III) and a saddle (branch IV). Analysis of the stability of these branches within the framework of the initial equations (80)

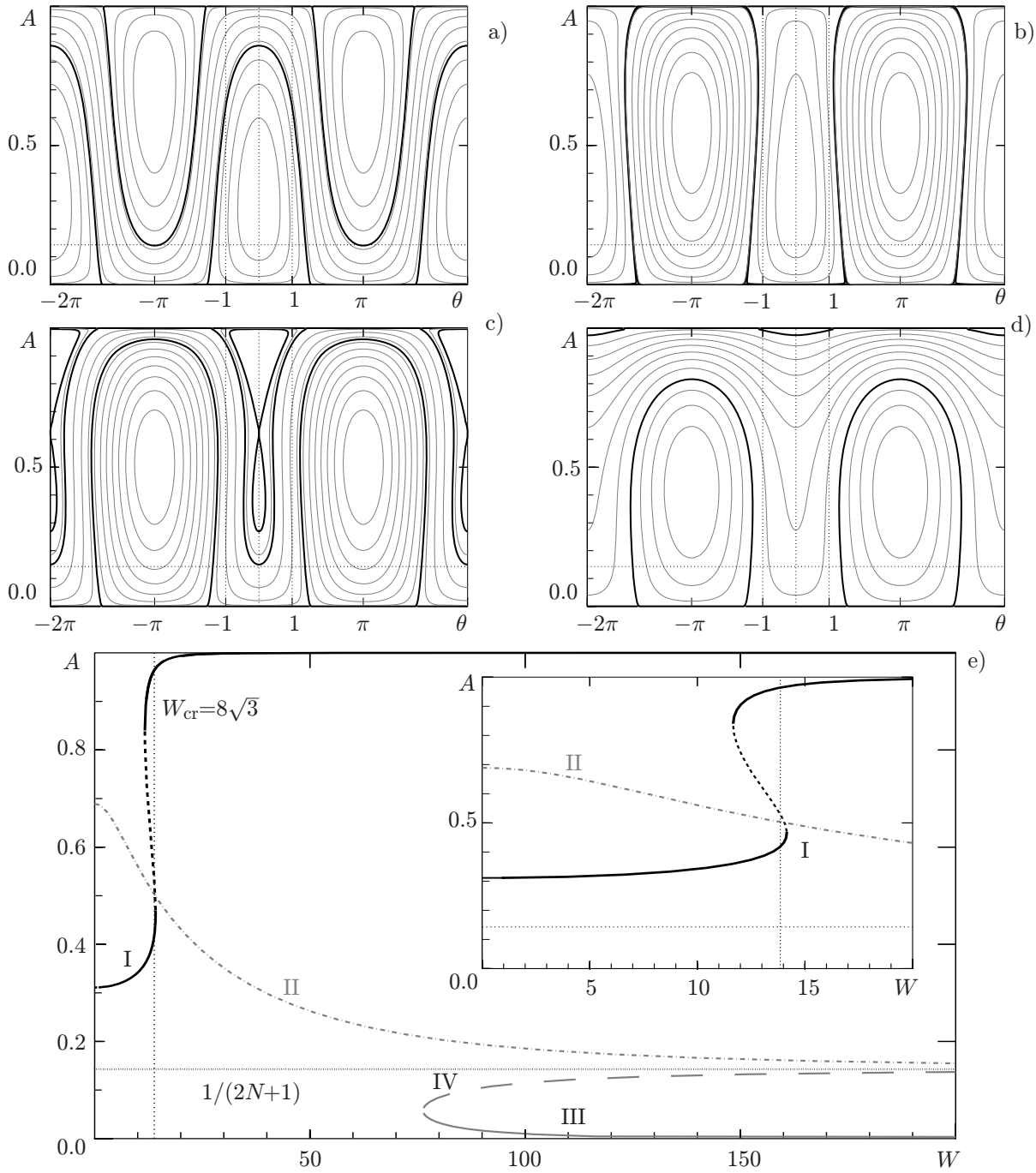

Fig. 14. Phase plane of Eqs. (86a) and (86b) with Eqs. (88) taken into account at different values of the energy W for the case $N = 3$, $\chi = 1$. The heavy lines mark the separatrices. The dotted line corresponds to the homogeneous distribution $|a| = |u_n|$. The equilibrium states depending on the energy W are shown in panel (*e*). The dashed line indicates the unstable equilibrium states.

shows that the only stable branch of the in-phase distribution of the solitons ($\theta_{\rm sol} = 0$) is I, similarly to the situation in the beam problem.

The jumpwise character of the variation in $A_{\rm I}$ at $W \approx W_{\rm cr}$ allows one to propose a method for self-compression of a laser pulse with an energy above the critical one, when the laser radiation is being trapped inside the central core [35, 36]. At $W < W_{\rm cr}$, the fraction of the energy in the central light guide $A_{\rm sol}$ is almost constant, which allows one to set $A \approx A_{\rm in} = 1/2 - 1/(2\sqrt{2N+1})$. At $W > W_{\rm cr}$, the wave field is

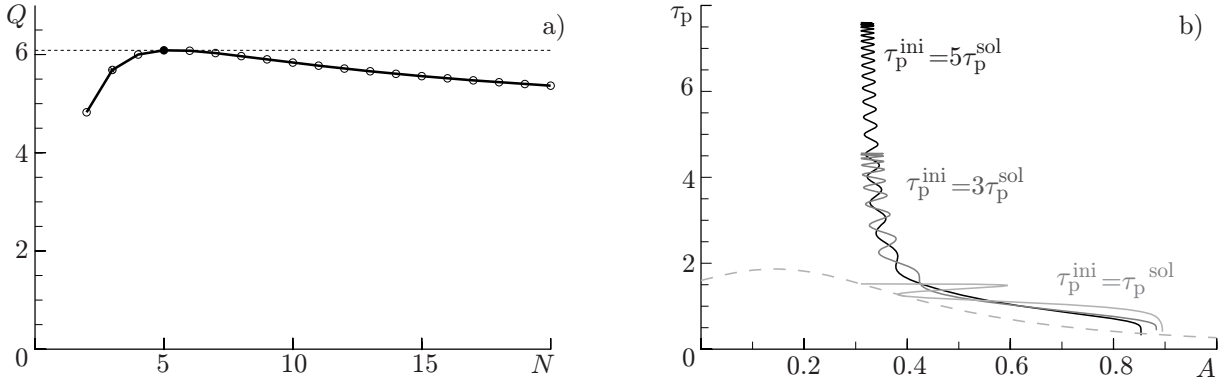

Fig. 15. (*a*) Degree of the wave packet compression calculated by formula (94) at $\eta_{\mathsf{est}} = 1$ and $A = A_{\mathsf{in}}$. (*b*) Duration (88) of the soliton (dashed line) and the dynamics of the wave packet parameters according to Eqs. (86) at $W = 15$ and different initial durations $\tau_{\mathrm{p}}^{\mathsf{ini}}$.

concentrated mainly in the central core ($A \approx 1$) and has the form of a light bullet with the duration (88), which is close to the duration of the NSE soliton of the same energy. The transition from one part of branch I to another happens almost with no energy loss in the hysteresis region $W \approx W_{\mathrm{cr}}$, so the degree of compression of the laser pulse is equal to $Q_* = 1/\left[A_{\mathrm{in}}^2 + (1 - A_{\mathrm{in}})^2/(2N)\right] \lesssim 6$ and depends only weakly on the number of light guides (Fig. 15*a*). The increase in the initial energy W at a fixed value $A = A_{\mathrm{in}}$ drives the initial distribution of the laser pulse farther and farther away from the hysteresis region. Correspondingly, the radiation trapping becomes possible for progressively smaller energy fraction $\eta \leq 1$.

For the efficient radiation trapping inside the central core, it is necessary to get in the small vicinity of the stable equilibrium state. Assuming that the length of the energy transfer to the center is equal to $1/(2\chi)$, we estimatethe variation $\delta\theta$ roughly from the formulas (86b) and (88) for $A \approx A_{\mathrm{in}}$,

$$|\delta\theta| \approx \frac{1}{2\chi}\frac{W^2}{48N^2}[(2N+1)A_{\mathrm{in}} - 1][2NA_{\mathrm{in}}^2 + (1 - A_{\mathrm{in}})^2].$$

Correspondingly, the condition of proximity to the target equilibrium state $|\delta\theta| \leq 1$ can be fulfilled only for the energies below [35, 36]

$$W_{\mathrm{lim}} \approx \frac{4N\sqrt{6\chi}}{\sqrt{[(2N+1)A_{\mathrm{in}} - 1][2NA_{\mathrm{in}}^2 + (1 - A_{\mathrm{in}}^2)]}}. \tag{91}$$

For example, for the parameter values $\chi = 1$ and $2N = 6$, the energy in the pulse is limited by $W \leq W_{\mathrm{lim}} \approx 26$, and the pulse duration should satisfy $\tau_{\mathrm{p}}^{\mathrm{out}} \geq 4/W_{\mathrm{lim}} \approx 0.15$.

The notion of the maximum energy allows one to predict the dynamics of the wave field for even greater initial energies. If the difference between the initial energy W and W_{lim} exceeds the critical energy W_{cr}, several less intense diverging pulses can be formed, and the laser pulse splits in the longitudinal direction for the energies

$$W \gtrsim W_{\mathrm{lim}} + W_{\mathrm{cr}} \approx 40. \tag{92}$$

This makes it possible to estimate the compression efficiency η. The estimate of the lower boundary of the efficiency, $\eta \geq \eta_{\mathrm{min}} = W_{\mathrm{cr}}/W$ is obtained from the requirement $W \geq W_{\mathrm{cr}}$ for the energy of the light bullet. Obviously, the efficiency near the hysteresis is close to 100%, i.e., $\eta \approx 1$ at $W = W_{\mathrm{cr}}$. We assume that the efficiency changes continuously as the total energy increases, and, at the total energy $W \simeq W_{\mathrm{lim}} + W_{\mathrm{cr}}$, two wave structures with the energy of the order of the critical value are formed in the splitting process. Then, the simplest approximation for the efficiency takes the form

$$\eta_{\mathrm{est}} \approx \frac{2W_{\mathrm{cr}}}{W + W_{\mathrm{cr}}}, \tag{93}$$

which is confirmed numerically. Altogether, this allows one to estimate the compression degree Q as the ratio of the initial ($\tau_{\rm p}$) and final ($\tau_{\rm p}^{\rm out}$) durations,

$$Q = \frac{\tau_{\rm p}}{\tau_{\rm p}^{\rm out}} \approx \eta_{\rm est} Q_* = \frac{\eta_{\rm est}}{A_{\rm in}^2 + (1 - A_{\rm in})^2/(2N)} \lesssim 6. \tag{94}$$

Thus, the use of soliton-like pulses with the energy $W \approx W_{\rm cr}$ allows compressing the pulse by 6 times with an energy efficiency of 100%. In this case, the change in the core number leads to only a slight variation in the compression degree (Fig. 15*a*).

The only possibility to raise the compression degree Q is to increase the initial duration of the wave packet $\tau_{\rm p}$ at a fixed total energy, i.e., to use the wave packet in the form (85) without the explicit relation (88) between the duration and the energy at an equilibrium point. Figure 15*b* shows the trajectories of the duration and the energy fraction in the central core for durations 3 and 5 times more than the optimal one (88). As seen, at the initial stage, the nonlinearity exceeds the medium dispersion significantly, and the duration of the wave packet decreases in accordance with the law $\mathrm{d}^2\tau_{\rm p}/\,\mathrm{d}z^2 \propto -W/\tau_{\rm p}^2$. In this case, the fraction of the energy in the central light guide is nearly constant ($A \approx A_{\rm in}$). As soon as the duration of the wave packet becomes comparable with the duration (88) of the found solution, the trapping to the central core occurs, accompanied by a decrease in the duration of the wave packet down to the value $4/(\eta W)$. The generalization of the expression for the compression degree is trivial in this case, $Q = \tau_{\rm p}/\tau_{\rm p}^{\rm out} \approx \eta Q_* W/W_0$. Here, for the sake of convenience, the energy

$$W_0 = \frac{4}{\tau_{\rm p}} \frac{1}{A_{\rm in}^2 + (1 - A_{\rm in})^2/(2N)} \leq W,$$

is defined, which corresponds to the initial duration $\tau_{\rm p}$ in accordance with formula (88).

The results of numerical simulation agree well with the obtained analytical estimates (92)–(94). Thus, this method of laser pulse self-compression in an MCF allows one to achieve significant shortening (by tens of times) of the laser pulse duration with an energy efficiency of more than 50% [35, 36]. And, the use of pulses with the energy close to the threshold one, $W_{\rm cr} = 8\sqrt{3}$, allows one to achieve a nearly 100% energy efficiency with the compression degree decreased by not more than two times.

7. EXPERIMENTAL STUDY OF THE NONLINEAR SUPPRESSION OF THE DISCRETE DIFFRACTION

This and the next sections present some of the experimental results that confirm good prospects for using fibers with coupled cores in design of laser systems. First, we studied thoroughly the effect of nonlinear suppression of discrete diffraction and demonstrated the possibilities of using this effect to compress and refine the ultrashort pulses from the low-intensity pedestal, i.e., to improve their contrast. The transfer of energy between the cores in arrays of coupled waveguides in the linear regime can be considered as a manifestation of the discrete diffraction effect [38]. In the nonlinear propagation regime, the discrete diffraction can be suppressed for high-power radiation, which leads to various spatiotemporal effects [39, 40] and can be used, e.g., to create a saturable absorber. We are aware of only few experimental works on the matter. Some features of nonlinear transmission were studied experimentally in the quartz [41] and chalcogenide [42] MCFs, as well as in the one-dimensional array of AlGaAs waveguides [43]. We have studied consistently the spatiotemporal dynamics of the high-power femtosecond pulses injected into one of the cores of the quartz MCF and undergoing the nonlinear suppression of the discrete diffraction. The experiment was performed with the use of the setup shown in Fig. 16*a* [44]. The radiation was produced by an erbium fiber laser system (I) that generated pulses at a wavelength of 1.56 μm with an energy of 0.4 μmJ and a duration of 370 fs. The structure of the seven-core quarts fiber used in the experiment is shown in the inset in Fig. 16*a*. The radiation of an adjustable power was injected into the central core of the fiber (II) and analyzed at the output using infrared camera (III), optical spectrum analyzer (IV), and the frequency-resolved optical gating (FROG) system (V).

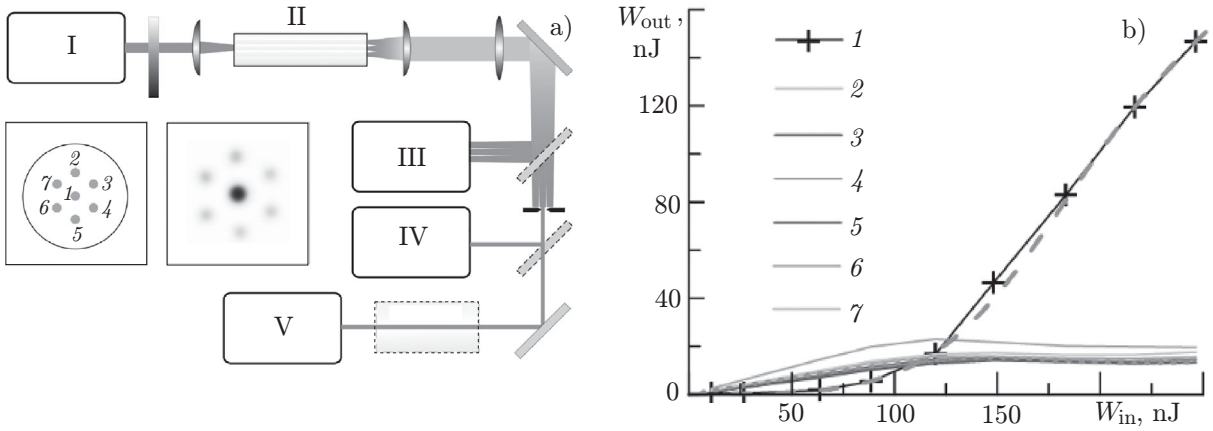

Fig. 16. (*a*) Experimental setup for studying the nonlinear pulse propagation in a seven-core fiber. The insets show the structure of the fiber and an example of the intensity profile at the fiber output. (*b*) The output pulse energy W_{out} in the cores as a function of the input energy W_{in}; the dashed and solid lines indicate the results of the numerical simulation and the measurements, respectively.

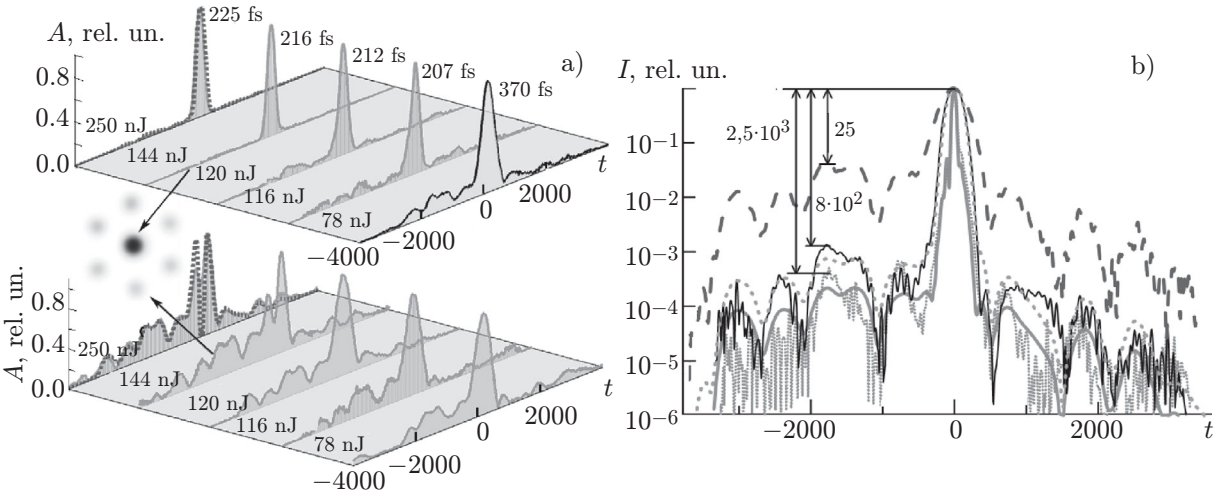

Fig. 17. (*a*) Measured (solid curves) and simulated (dashed curves, only for the maximum energy) pulse profiles at the MCF output for different energies (central core and one of the side cores in the top and bottom panels, respectively. (*b*) Measurement and simulation of the pulse compression and contrast enhancement: the measured input pulse (dashed black line), the measured and simulated pulse at the output from the central core (solid black line and dashed gray line, respectively), and the measured and simulated compressed pulse (dashed gray line and solid gray line, respectively).

The fiber length was chosen to be equal to the half-length of the linear transfer length. Therefore, a great fraction of the radiation flowed to the side cores at a low input power. As the input power increases, the nonlinear phase incursion leads to a decrease in the energy transfer (suppression of the discrete diffraction), which results in the radiation trapping in the central core in the high-power limit. In the experiment, it was manifested as an increase in the energy fraction in the central core as the energy of the injected radiation grew (Fig. 16*b*). The measurement results were compared with the numerical simulation on the basis of the coupled generalized nonlinear Schrödinger equations. The comparison demonstrated good agreement for both the integral characteristics (Fig. 16*b*) and the temporal pulse profiles (Fig. 17*a*).

The results presented in Fig. 17*a* show that the highest-power central part of the ultrashort pulse stays in the central core, whereas the radiation of the extended pulse pedestal flows to the side cores improving the pulse contrast significantly. A high-power pulse propagating in the trapping regime in the central core

undergoes strong phase self-modulation and spectral widening. Pulses having a duration of 53 fs and a peak power of about 2.1 MW, which exceeds the peak power of the input pulse by almost four times, were obtained through the compensation of the nonlinear phase in a linear dispersive element (a 12.5 cm long glass rod). As a result of nonlinear profiling in the MCF and an increase in the peak power during compression, the pulse contrast (the ratio between the peak and pedestal intensities) was improved by two orders of magnitude (Fig. 17*b*). Thus, a system was developed generating high-quality 53-fs pulses with the submicrojoule energy level and the megawatt level of the peak power. This can be regarded as one of the first demonstrations of the experimental application of MCFs in the field of developing high-power femtosecond laser systems.

8. RADIATION INPUT TO AND OUTPUT FROM MCF

An important issue of practical MCF application for handling high-power radiation is the development of methods for efficient injection of radiation generated by the seed source to the fiber cores, as well as for conversion of the output radiation into a single beam having acceptable quality. In the case of an MCF with coupled cores, it is necessary to use a converter from the quasi-Gaussian mode (the mode of the fiber of the seed source) to the required MCF supermode. Modern technologies of controlling the spatial radiation structure allows one to solve these problems. One of such methods is based on the use of spatial light modulators (SLMs). A typical modulator is a pixel matrix with a resolution of the order of 1000×1000 where control of the radiation phase is possible in each pixel. Using such devices and applying the methods of Fourier optics, one can synthesize the required amplitude-phase structure of the supermode at the input with sufficient accuracy and an acceptable loss level, as it was done, e.g., in [6, 45, 46]. Technically, after testing the scheme with the adjustable modulator one may replace it with a fixed phase mask which can be manufactured using lithographic methods and may be used to achieve high power levels. One should also mention the possibility to create monolith mode converters based on special MCFs with interacting cores. For example, in an MCF with one central core and a ring of cores, the radiation injected into the central core is transferred to the cores on the ring at a certain length of the MCF, and the in-phase mode is effectively synthesized. In order to convert the in-phase mode to the out-of-phase one, one may use an additional fiber section with the ring arrangement of noninteracting cores with the even and odd cores having slightly different effective refractive indices providing the required phase incursion. All the sections of the fiber can be welded together by using the available welding techniques. Monolith fiber devices are also known in which the array of individual input fibers is fused or glued together (after the coatings of the individual fibers have been etched to the required diameter) so that the structure of the array cores correspond to the MCF cores [47]. These methods can be used successfully to inject radiation in an MCF amplifier while the input power is not too high. The task of outputting high-power amplified radiation requires a transformation of the MCF supermode into one output beam in free space. This can be done by means of optical schemes similar to those used for coherent summation of optical beam arrays. Moreover, the out-of-phase arrays of the beams at the output of a rectangular MCF can be transformed readily to a single beam with an efficiency exceeding 90% [48]. This method was tested experimentally for transformation of the out-of-phase MCF mode to one beam with sufficiently high quality ($M^2 < 1.3$) [49]. It is more difficult to convert the out-of-phase mode of the ring structure to a single beam. Nevertheless, we proposed and tested numerically the optical scheme, which enables this conversion with theoretically achievable efficiency at a level of 80% [50]. Note that these schemes can be also used in the reverse direction to convert one beam to an array of beams for injection into an MCF.

9. EXPERIMENTAL STUDIES OF SELECTIVE EXCITATION AND AMPLIFICATION OF THE OUT-OF-PHASE SUPERMODE

We performed a series of experimental studies on the possibility to excite, transport, and amplify the out-of-phase modes considered above. We started with fibers having the ring core structure. An active fiber with six ytterbium-doped cores was developed for this purpose [45]. Single-core blanks for active cores

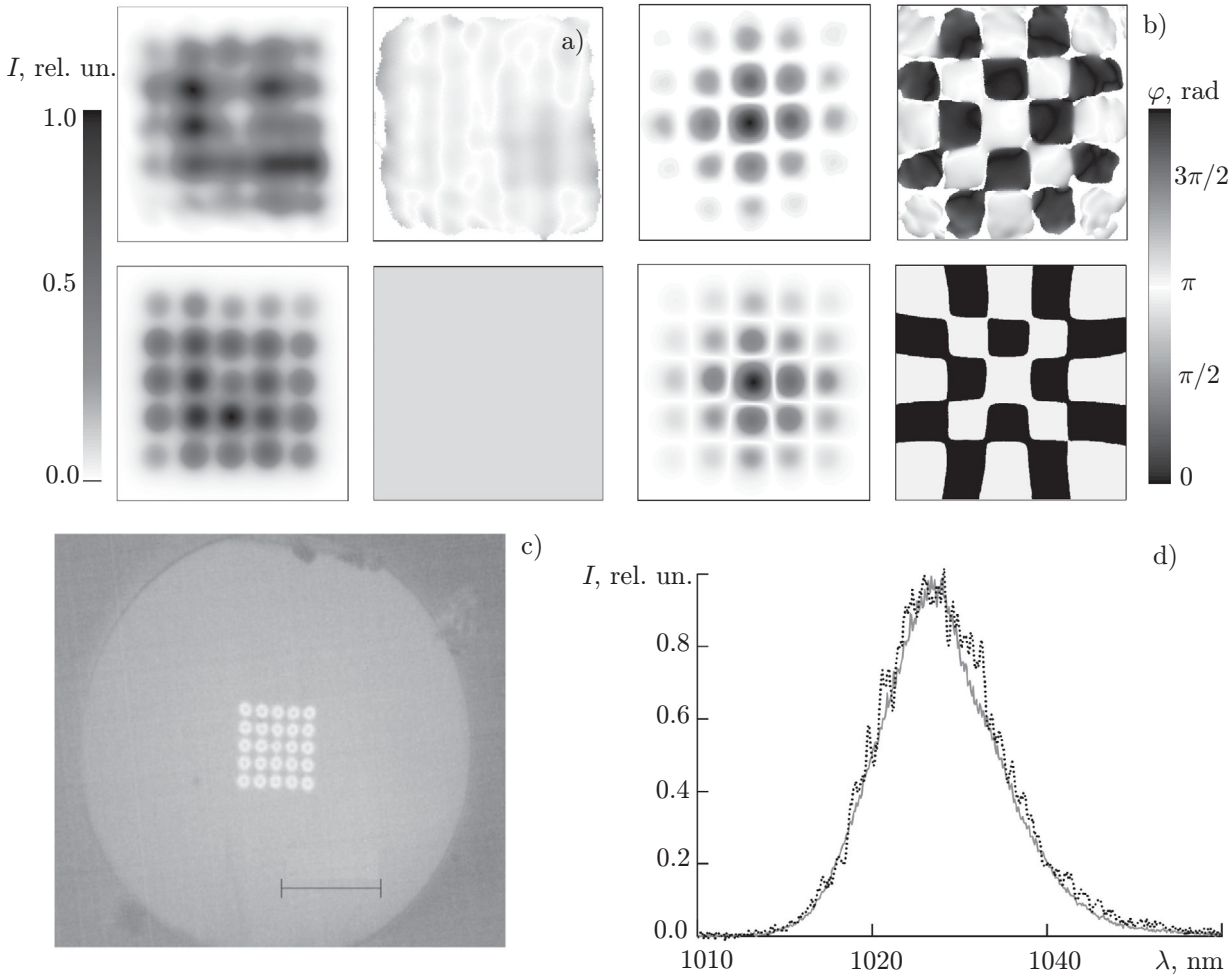

Fig. 18. Propagation of supermodes in a fiber with the square core matrix: the measured (upper row) and calculated (lower row) profiles of the intensity (left-hand columns) and phase (right-hand columns) of the in-phase (*a*) and out-of-phase (*b*) supermodes. (*c*) Microphotograph of the transverse cross section of the fiber (the length of the scale bar is 50 μm). (*d*) Spectra of the radiation at the input (solid gray line) and output (dashed black line) of the MCF.

were manufactured at the G. G. Devyatykh Institute of Chemistry of High-Purity Substances of the Russian Academy of Sciences with the use of modified chemical vapor deposition (MCVD) technique. The MCF was assembled and drawn by the collaborators of the Fiber Optics Research Center of the Russian Academy of Sciences and the Prokhorov General Physics Institute of the Russian Academy of Sciences. An MCF blank was a quartz rod with six drilled holes, in which single-core blanks were inserted. The coatings of the blanks were etched in advance almost down to the central cores; as a result, gaps between the cores in the MCF were ensured to be small. The central part of the manufactured MCF imaged by an electron microscope is presented in the inset in Fig. 18*a*. The quartz cladding of the MCF with a diameter of 100 μm was surrounded by the second polymer cladding with a lower refraction index, which enabled propagation of the multimode pumping radiation.

The experimental setup shown in Fig. 19*a* was developed for studying the pulse propagation and amplification in the MCF. A hybrid erbium-ytterbium system *1* was used as a radiation source [51, 52]. The system generated pulses with a repetition rate adjustable from 1 to 16 MHz at a central wavelength of 1.03 μm. The scheme based on an SLM *2* allowed synthesizing six beams with adjustable phases between them and was used for efficient injection of the radiation into the MCF *4* . The fiber was pumped by a multimode laser diode *3* via a dichroic mirror. The mode composition of the radiation at the MCF

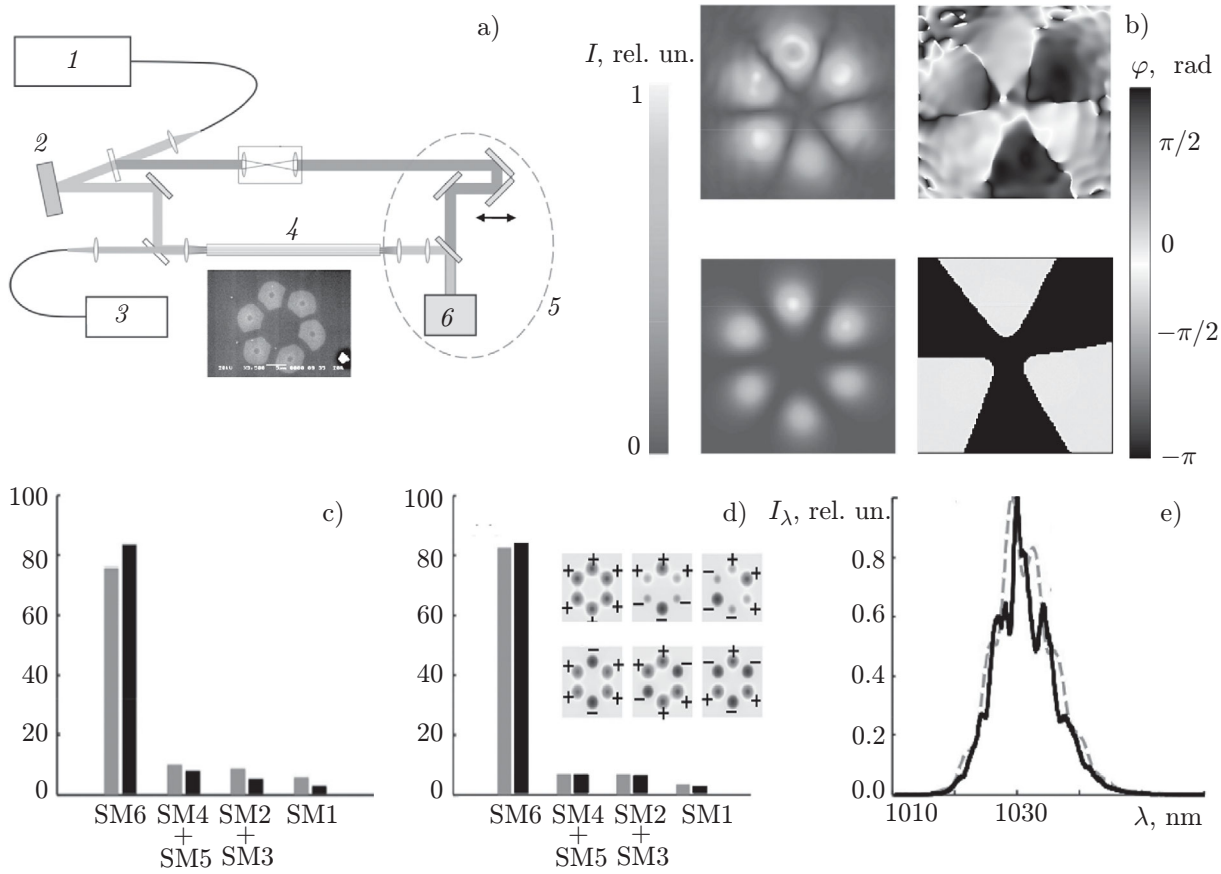

Fig. 19. (*a*) Setup for studying the excitation and amplification of the supermodes in a six-core ytterbium light guide. The inset shows the central part of the fiber imaged by an electron microscope. (*b*) The measured (upper row) and calculated (lower row) profiles of the amplitude (left-hand column) and phase (right-hand column) of the out-of-phase supermode. The measured (*c*) and calculated (*d*) mode composition of the radiation at the MCF output in the cases pumping turned off (gray color) and on (black color) (as a percentage, for the supermodes). The inset shows the structures of the MCF supermodes SM1–SM6. (*e*) The spectra at the MCF output (the dependences of the spectral intensity I_λ on the wavelength λ).

output was analyzed by using the interferometric scheme *5*. In this scheme, part of the radiation from the seed source passes through an adjustable delay line and is combined then with the image of the output end of the fiber at the infrared camera *6*. If the delay corresponds to the group delay of one of the fiber supermodes, an interference pattern is observed at the camera, allowing one to retrieve the amplitude and phase of the mode field. The radiation input was optimized by using a special iteration algorithm based on the gradient descent method where the data of the mode composition at each iteration were taken into account, and the phase mask at the SLM was adjusted. Selective excitation of the out-of-phase mode was achieved with the share of the mode in the output radiation exceeding 90%. The signal power was equal to 0.9 W in the amplification regime at a maximum pump power of 12 W. This corresponded to an energy of 0.9 μJ and a peak power of about 18 kW at the minimum repetition rate. The diagrams which were measured or obtained by numerical simulation and present the mode content of the radiation are shown in Figs. 19*c* and 19*d*. The field structures of the six supermodes supported by an ideal MCF are shown in the inset in Fig. 19*d*. The experimental scheme made it possible to separate the contribution of the out-of-phase supermode SM6, in-phase supermode SM1, and pairs of the degenerate supermodes: SM2+SM3 and SM3+SM4. The contribution of the out-of-phase supermode in the amplified radiation exceeded 80%. No significant distortions of the spectrum were observed from the amplification, indicating that such an amplifier can be applied in systems for amplification of ultrashort chirped pulses (Fig. 19*e*).

We simulated numerically the radiation amplification using the three-dimensional code taking into account the actual structure of the transverse cross section of the fiber and the imperfect injection of the radiation into the MCF. The comparison of the results yielded by the experiments and the simulation demonstrated, in particular, the coincidence of the measured and calculated mode structures and also confirmed weak changes in the mode composition in the amplification regime (Fig. 19*d*), specifically, a slight increase in the fraction of the out-of-phase mode due to a greater overlap integral between this mode and the doped cores.

Thus, the experiment demonstrated the possibility of selective excitation and stable amplification of chirped pulses with the transverse structure of the out-of-phase supermode in a fiber with the ring arrangement of the cores. The numerical simulations based on three-dimensional numerical codes taking into account the spatial distributions of the gain and the refraction index [53]) showed that the total peak power of about 1 MW is achievable in a fiber that can be produced from the same blank but has a diameter of 1.5 times larger, with the intensity flattening over the cores observed [45].

The next experiment was performed in a fiber with the square core matrix. The fiber with a square 5×5 core matrix was developed and manufactured so that the possibility of excitation and propagation of the out-of-phase supermode could be verified. We used an experimental system similar to that shown in Fig. 19*a* with some modifications for the fibers with the square core matrix. In particular, the way of synthesizing the field at the MCF input end was changed: Specifically, we used the transfer of the SLM-plane image to the fiber end with an intermediate spatial filter [46]. This allowed us to obtain the required phase distribution directly on the SLM matrix without the use of the Fourier transform. By specifying various field distributions at the MCF input and analyzing the mode composition at the output, we identified several MCF supermodes, in particular, the in-phase and out-of-phase modes shown in Fig. 18*a* and 18*b*. We also measured the propagation constants of these modes; the measurement results agreed well with the results of the numerical simulation of the supermodes for this MCF with the actual structure of its cores taken into account. The measured amplitude and phase profiles of the supermodes also were in good agreement with the calculated distributions. After optimization of the input, the contribution of the out-of-phase supermode at the fiber output was 88%. It should be emphasized that after the initial adjustment, the mode composition and the amplitude and phase ratios between the fields in the cores remained constant without any feedback system. Due to this, this system compares favorably with an array of independent fiber channels. The radiation spectrum measured in one of the central cores at the MCF output was identical to the spectrum of the initial signal, which again indicates the good mode purity of the radiation and the absence of radiation flow into other modes.

Thus, in our experiments, we managed to excite selectively the out-of-phase mode in a fiber with a square core matrix and measure its phase and amplitude profiles, as well as demonstrate the propagation of broadband chirped radiation with the transverse structure corresponding to this mode.

It was impossible to achieve experimentally a propagation regime with the intensity flattening over the cores since the radiation power available at the time of the experiment was insufficient. However, the possibility of this regime was confirmed by numerical simulation [46]. The possibilities of raising the peak power further are related to combining the concepts of tapered and multicore fibers. The fiber amplifier proposed in [50] is based on a monolith fiber with an array of coupled cores and a diameter increasing from the input to the output. In such light guides, radiation can be injected efficiently without excitation of undesirable modes even if the synthesis of the required input field is not precise. At the same time, an adiabatic increase in the area of the fundamental mode with approaching the output conduces to decreasing the undesirable influence of the nonlinear effects. The three-dimensional numerical simulation using the method optimized for strongly chirped pulses [54] demonstrated that, the total peak power of about 50 MW is achievable in a MCF with a square array of 11×11 cores when the out-of-phase mode is amplified.

A distinctive feature of the out-of-phase mode in a square core matrix is that high-efficiency coherent summation of the radiation at the MCF output is possible with the method proposed in [48]. The summation efficiency of the out-of-phase supermode in the experiment reached 81% [49].

It should be also noted that the switching between different supermodes can be performed by means of changing the spatial structure of radiation enables control of the group velocity dispersion in the MCF. It was demonstrated experimentally in [55] that in quartz MCFs, the zero dispersion point of the out-of-phase mode in quartz MCFs shifts toward shorter wavelengths from the material zero of the dispersion. This property can be significant in the context of implementation of many interesting regimes of radiation propagation in the spectral region in the vicinity of 1 μm, where there are high-power radiation sources and active ytterbium fibers available, but it is very difficult to advise abnormal dispersion of the group velocities.

10. CONCLUSIONS

The presented review of modern studies of laser radiation self-action in MCFs with weakly coupled cores allows one to make certain practical proposals. The primary objective of using MCFs was to abate the filamentation instability by using the spatial modulation of the refractive index and to secure the possibility to transport coherent wave beams with the powers exceeding the critical self-focusing power. However, almost all wide distributions of the wave field proved to be subject to discrete filamentation instability which led either to self-trapping of the radiation (discrete analog of the collapse) or to stochastic dynamics, which disrupts the coherence of the wave packet. The only exception were the out-of-phase supermodes, i.e., the wave field distributions over all fiber cores that have the maximum propagation constant so that their rescattering to other distributions is energetically unfavorable. This work presents the out-of-phase supermodes for several core configurations (a ring, a line, a square matrix, and a hexagonal structure) and the results of the experimental studies which demonstrated their implementability and stability. The presence of such stable out-of-phase supermodes makes it possible to handle wave beams with powers up to N critical self-focusing powers, where N is the number of cores in the MCF. Moreover, the use of external phase synchronization allows an additional several-fold increase in the achievable power of the coherent wave beam. This reveals wide prospects for design of high-power fiber systems of multimegawatt power levels.

This work was supported by the Russian Science Foundation (Project No. 23–12–00248).

REFERENCES

1. G. Mourou, T. Tajima, M. N. Quinn, et al., *Nucl. Instrum. Methods Phys. Res. Sect. A*, **740**, 17–20 (2014). https://doi.org/10.1016/j.nima.2013.10.041
2. G. Mourou, B. Brocklesby, T. Tajima, and J. Limpert, *Nature Photon.*, **7**, No. 4, 258–261 (2013). https://doi.org/10.1038/nphoton.2013.75
3. M. Müller, M. Kienel, A. Klenke, et al., *Opt. Lett.*, **41**, No. 15, 3439–3442 (2016). https://doi.org/10.1364/OL.41.003439
4. J. Bourderionnet, C. Bellanger, J. Primot, and A. Brignon, *Opt. Express*, **19**, No. 18, 17053–17058 (2011). https://doi.org/10.1364/OE.19.017053
5. A. Klenke, M. Müller, H. Stark, et al., *IEEE J. Sel. Topics Quantum Electron.*, **24**, No. 5, 2808540 (2018). https://doi.org/10.1109/JSTQE.2018.2808540
6. L. P. Ramirez, M. Hanna, G. Bouwmans, et al., *Opt. Express*, **23**, No. 5, 5406–5416 (2015). https://doi.org/10.1364/OE.23.005406
7. A. Klenke, M. Müller, H. Stark, et al., *Opt. Lett.*, **43**, No. 7, 1519–1522 (2018). https://doi.org/10.1364/OL.43.001519
8. A. M. Ortiz and R. L. Saez, in: F. Xu and C. Mou, eds., *Selected Topics on Optical Fiber Technologies and Applications*, IntechOpen, Rijeka (2018), pp. 63–102. https://doi.org/10.5772/intechopen.72458
9. R. Mercy Kingsta and R. Shantha Selvakumari, *Optik*, **199**, 163341 (2019). https://doi.org/10.1016/j.ijleo.2019.163341

10. M. Koshiba, K. Saitoh, and Y. Kokubun, *IEICE Electron. Express*, **6**, No. 2, 98–103 (2009). https://doi.org/10.1587/elex.6.98
11. K. Saitoh and S. Matsuo, *J. Lightw. Technol.*, **34**, No. 1, 55–66 (2016). https://doi.org/10.1109/JLT.2015.2466444
12. A. A. Balakin, A. G. Litvak, V. A. Mironov, and S. A. Skobelev, *Phys. Rev. A*, **94**, No. 6, 063806 (2016). https://doi.org/10.1103/PhysRevA.94.063806
13. Y. S. Kivshar and S. K. Turitsyn, *Phys. Rev. E*, **49**, No. 4, R2536–R2539 (1994). https://doi.org/10.1103/PhysRevE.49.R2536
14. A. B. Aceves, G. G. Luther, C. De Angelis, et al., *Phys. Rev. Lett.*, **75**, No. 1, 73–76 (1995). https://doi.org/10.1103/PhysRevLett.75.73
15. H. S. Eisenberg, Y. Silberberg, R. Morandotti, et al., *Phys. Rev. Lett.*, **81**, No. 16, 3383–3386 (1998). https://doi.org/10.1103/PhysRevLett.81.3383
16. A. A. Balakin, A. G. Litvak, V. A. Mironov, and S. A. Skobelev, *Laser Phys.*, **28**, No. 4, 045401 (2018). https://doi.org/10.1088/1555-6611/aaa115
17. A. A. Balakin, S. A. Skobelev, E. A. Anashkina, et al., *Phys. Rev. A*, **98**, No. 4, Art. no. 043857 (2018). https://doi.org/10.1103/PhysRevA.98.043857
18. H. Tünnermann and A. Shirakawa, *Opt. Express*, **23**, No. 3, 2436–2445 (2015). https://doi.org/10.1364/OE.23.002436
19. A. A. Balakin, S. A. Skobelev, and A. G. Litvak, *EPL*, **132**, No. 5, 54001 (2020). https://doi.org/10.1209/0295-5075/132/54001
20. A. A. Balakin, S. A. Skobelev, A. V. Andrianov, et al., *Opt. Lett.*, **45**, No. 12, 3224–3227 (2020). https://doi.org/10.1364/OL.392607
21. A. A. Balakin, S. A. Skobelev, A. V. Andrianov, et al., *Opt. Lett.*, **46**, No. 2, 246–249 (2021). https://doi.org/10.1364/OL.401914
22. A. A. Balakin, A. G. Litvak, and S. A. Skobelev, *Phys. Rev. A*. **102**, No. 2, 023527 (2020). https://doi.org/10.1103/PhysRevA.102.023527
23. S. A. Skobelev, A. A. Balakin, E. A. Anashkina, et al., *Phys. Rev. A*, **104**, No. 2, 023522 (2021). https://doi.org/10.1103/PhysRevA.104.023522
24. V. I. Talanov, *Izv. Vyssh. Uchebn. Zaved., Radiofiz.*, **7**, No. 3, 564–565 (1964).
25. V. I. Talanov, *JETP Lett.*, **2**, No. 5, 138–141 (1965).
26. A. G. Litvak and V. I. Talanov, *Radiophys. Quantum Electron.*, **10**, No. 4, 296–302 (1967). https://doi.org/10.1007/BF01041026
27. V. I. Bespalov and V. I. Talanov, *JETP Lett.*, **3**, No. 12, 307–310 (1966).
28. S. N. Vlasov, V. A. Petrishchev, and V. I. Talanov, *Radiophys. Quantum Electron.*, **14**, No. 9, 1062–1070 (1971). https://doi.org/10.1007/BF01029467
29. E. W. Laedke, K. H. Spatschek, S. K. Turitsyn, and V. K. Mezentsev, *Phys. Rev. E*, **52**, No. 5, 5549–5554. (1995) https://doi.org/10.1103/PhysRevE.52.5549
30. A. B. Aceves, G. G. Luther, C. De Angelis, et al., *Opt. Fiber Technol.*, **1**, 244–246 (1995). https://doi.org/10.1006/ofte.1995.1015
31. G. P. Agrawal, *Nonlinear Fiber Optics*, Academic Press, London (2019). https://doi.org/10.1016/G2018-0-01168-8
32. S. Tzortzakis, L. Sudrie, M. Franco, et al., *Phys. Rev. Lett.*, **87**, No. 21, 213902 (2001). https://doi.org/10.1103/PhysRevLett.87.213902

33. A. A. Balakin, A. G. Litvak, and S. A. Skobelev, *Phys. Rev. A*, **100**, No. 5, 053834 (2019). https://doi.org/10.1103/PhysRevA.100.053834

34. S. A. Skobelev, A. A. Balakin, E. A. Anashkina, et al., *Phys. Rev. A*, **104**, No. 3, 033518 (2021). https://doi.org/10.1103/PhysRevA.104.033518

35. A. A. Balakin, A. G. Litvak, and S. A. Skobelev, *Phys. Rev. A*, **100**, No. 5, 053830 (2019). https://doi.org/10.1103/PhysRevA.100.053830

36. A. A. Balakin, S. A. Skobelev, A. V. Andrianov, et al., *Opt. Lett.*, **44**, No. 20, 5085–5088 (2019). https://doi.org/10.1364/OL.44.005085

37. A. A. Balakin, S. A. Skobelev, E. A. Anashkina, et al., *Phys. Rev. A*, **98**, No. 4, 043857 (2018). https://doi.org/10.1103/PhysRevA.98.043857

38. D. N. Christodoulides and R. I. Joseph, *Opt. Lett.*, **13**, No. 9, 794–796 (1988). https://doi.org/10.1364/OL.13.000794

39. S. Minardi, F. Eilenberger, Y. V. Kartashov, et al., *Phys. Rev. Lett.*, **105**, No. 26, 263901 (2010). https://doi.org/10.1103/PhysRevLett.105.263901

40. I. S. Chekhovskoy, A. M. Rubenchik, O. V. Shtyrina, et al., *Phys. Rev. A*, **94**, No. 4, 043848 (2016). https://doi.org/10.1103/PhysRevA.94.043848

41. T. F. S. Büttner, D. D. Hudson, E. C. Mägi, et al., *Opt. Lett.*, **37**, No. 13, 2469–2471 (2012). https://doi.org/10.1364/OL.37.002469

42. S. Minardi, G. Cheng, C. D'Amico, and R. Stoian, *Opt. Lett.*, **40**, No. 2, 257–259 (2015). https://doi.org/10.1364/OL.40.000257

43. D. D. Hudson, K. Shish, T. R. Schibli, et al., *Opt. Lett.*, **33**, No. 13, 1440–1442 (2008). https://doi.org/10.1364/ol.33.001440

44. A. V. Andrianov, N. A. Kalinin, M. Yu. Koptev, et al., *Opt. Lett.*, **44**, No. 2, 303–306 (2019). https://doi.org/10.1364/OL.44.000303

45. A. V. Andrianov, N. A. Kalinin, E. A. Anashkina, et al., *J. Lightw. Technol.*, **38**, No. 8, 2464–2470 (2020). https://doi.org/10.1109/JLT.2020.2966025

46. N. A. Kalinin, E. A. Anashkina, O. N. Egorova, et al., *Photonics*, **8**, No. 8, 314 (2021). https://doi.org/10.3390/photonics8080314

47. J. Xiong, L. Ma, Y. Shi, et al., *IEEE Photon. J.*, **14**, No. 4, 7146805 (2022). https://doi.org/10.1109/JPHOT.2022.3198087

48. A. Andrianov, N. Kalinin, E. Anashkina, and G. Leuchs, *Opt. Lett.*, **45**, No. 17, 4774–4777 (2020). https://doi.org/10.1364/OL.391259

49. N. A. Kalinin, E. A. Anashkina, G. Leuchs, and A. V. Andrianov, *Opt. Express*, **30**, No. 2, 1013–1020 (2022). https://doi.org/10.1364/OE.446794

50. A. V. Andrianov, S. A. Skobelev, A. A. Balakin, et al., *IEEE Photon. J.*, **14**, No. 1, 1505606 (2022). https://doi.org/10.1109/JPHOT.2021.3135349

51. A. Andrianov, E. Anashkina, S. Muravyev, and A. Kim, *Opt. Lett.*, **35**, No. 22, 3805–3807 (2010). https://doi.org/10.1364/OL.35.003805

52. A. V. Andrianov, E. A. Anashkina, S. V. Muravyev, and A. V. Kim, *Quantum Electron.*, **43**, No. 3, 256–262 (2013). https://doi.org/10.1070/QE2013v043n03ABEH015132

53. A. Andrianov, E. Anashkina, A. Kim, et al., *Opt. Express*, **22**, No. 23, 28256–28269 (2014). https://doi.org/10.1364/OE.22.028256

54. A. Andrianov, A. Szabo, A. Sergeev, et al., *Opt. Express*, **24**, No. 23, 25974–25982 (2016). https://doi.org/10.1364/OE.24.025974

55. A. V. Andrianov, N. A. Kalinin, and E. A. Anashkina, *Laser Phys. Lett.*, **18**, No. 12, 125104 (2021). https://doi.org/10.1088/1612-202X/ac3516